PROJECT DELIVERABLE

Project acronym: **BioBarr**

Project title: **New bio-based food packaging materials with enhanced barrier properties – BioBarrier**

Grant Agreement number: *745586*

Del. no.	*Deliverable title*	*WP no.*	*Lead beneficiary*	*Nature*	*Dissemination level*	*Due date of deliverable*
8.4	One scientific Open Access article	8	TCA	ORDP: Open Research Data Pilot	Public	31/05/2021 – M48

Actual submission date: 28/05/2021 – M48

Document information

Authors
Marianna Faraldi, TCA, Italy
Mikolaj Owsianiak, DTU, Denmark

Project co-ordinator:
Mr Raffaello Prugger
Tecnoalimenti S.C.p.A.
Phone: +39 02 67077370
Fax: +39 02 67077405
E-mail: r.prugger@tecnoalimenti.com

Work-package 8 Leader
Mrs Marianna Faraldi
Organisation: Tecnoalimenti Scpa
Address: Via Gustavo Fara, 39 20124 Milano, Italy
Phone: +39 02 67077370
E-mail: m.faraldi@tecnoalimenti.com

Project funding
Grant Agreement number: 745586 — BioBarr — H2020-BBI-JTI-2016/H2020-BBI-JTI-2016

Table of contents

1. Introduction

Two scientific open access articles have been published until 31 May 2021. They are outcomes of WP7 Process-based life cycle assessment (LCA) and cost-benefit analysis (CBA). The two articles are:

Fabbri, S., Hauschild, M.Z., Lenton, T.M., Owsianiak, M., 2021. Multiple Climate Tipping Points Metrics for Improved Sustainability Assessment of Products and Services. Environ. Sci. Technol. 55, 2800–2810. https://doi.org/10.1021/acs.est.0c02928

Vea, E.B., Fabbri, S., Spierling, S., Owsianiak, M., 2021. Inclusion of multiple climate tipping as a new impact category in life cycle assessment of polyhydroxyalkanoate (PHA)-based plastics. Sci. Total Environ. 788, 147544. https://doi.org/10.1016/j.scitotenv.2021.147544

Fabbri et al. (2021) is an outcome of Task 7.3. It presents a new life cycle impact assessment method developed to improve assessment of climate change mitigation potential of bioplastics. The new method is based on new GHG emission metrics, the multiple climate tipping points potentials (MCTP), which covers 13 projected tipping points and incorporates the effect that the crossing of a given tipping point has on accelerating the crossing of other tipping points (including through surface albedo change mechanism).

Vea et al. (2021) presents scientific outcomes of Tasks 7.1 and 7.2. They applied the method presented in Fabbri et al. (2021) in process-based life cycle assessment of PHA-based plastics with improved barrier properties. Comparisons were made between PHA production at pilot and large scales. Multiple climate tipping was found to be a relevant impact category for LCA of PHA.

The two articles are presented in the Appendix 1.

2. Open access and data management

The data presented in the two articles are openly available to the public. They are assigned a digital object identifier (DOI) making the data findable and citable, including relevant metadata records. Metadata for underlying GHG emission metrics and model files are provided as supporting information to the articles. They contain relevant information (e.g., author, date, version, software to open the model file, description of what the model does and output it provides).

Appendixes

Appendix 1 – open access publications

Environmental Science & Technology

pubs.acs.org/est

Article

Multiple Climate Tipping Points Metrics for Improved Sustainability Assessment of Products and Services

Serena Fabbri,* Michael Z. Hauschild, Timothy M. Lenton, and Mikołaj Owsianiak

Cite This: *Environ. Sci. Technol.* 2021, 55, 2800–2810

Read Online

ACCESS | Metrics & More | Article Recommendations | Supporting Information

ABSTRACT: Mounting evidence indicates that climate tipping points can have large, potentially irreversible, impacts on the earth system and human societies. Yet, climate change metrics applied in current sustainability assessment methods generally do not consider these tipping points, with the use of arbitrarily determined time horizons and assumptions that the climate impact of a product or service is independent of emission timing. Here, we propose a new method for calculating climate tipping characterization factors for greenhouse gases (carbon dioxide, methane, and nitrous oxide) at midpoint. It covers 13 projected tipping points, incorporates the effect that the crossing of a given tipping point has on accelerating the crossing of other tipping points, and addresses uncertainties in the temperature thresholds that trigger the tipping points. To demonstrate the added value of the new metric, we apply it to emissions stemming from end-of-life of plastic polymers and compare them with commonly used metrics. This highlights the need to consider climate tipping in sustainability assessment of products and services.

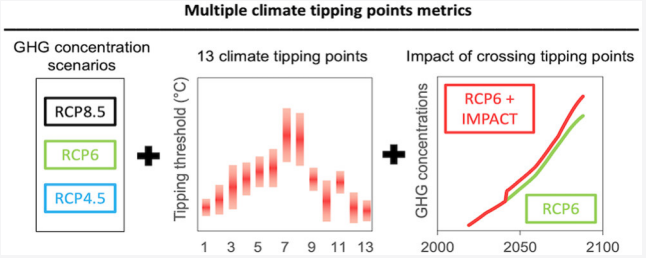

INTRODUCTION

There are several elements of the earth system that could pass a tipping point within this century and trigger large abrupt, potentially irreversible changes.[1] Examples of tipping elements include Arctic summer sea ice, the Atlantic thermohaline circulation, and the El Niño-southern oscilation.[2] The crossing of these elements may be one of the most dangerous consequences of human-induced climate change.[3] From the economic perspective only, Cai et al. showed an eight time increase in monetary costs per 1 tonne of carbon dioxide emitted, when compared to the costs without considering the tipping.[4] These findings stress the need for consideration of climate tipping elements when developing metrics of climate impact for improved environmental sustainability assessment of products and services.

Life cycle assessment (LCA) is a tool that is often used to address the environmental sustainability of products and systems.[5] In LCA, the climate change impacts of a product or service are traditionally quantified using global warming potentials (GWP)[6] as characterization factors (CF), representing the impact per unit of emission. Amounts of individual greenhouse gases (GHG) that can be attributed to a specific product or service are first summed up and then multiplied by a GHG-specific GWP; the resulting indicator scores added. The sum represents the climate change impact score (also referred to as carbon footprint)[7] and expresses the potential contribution of a product or service to change radiative forcing (not the actual warming) over a defined time horizon, typically over 100 years. The procedure for calculating impact scores is the same for all other midpoint indicators of climate change (where midpoint refers to the location of the indicator in the cause-effect chain linking emission inventories with final damage caused to environment or human health). For another midpoint indicator, global temperature change, the global temperature change potential (GTP)[8] is used and the resulting impact scores indicate the potential contribution of a product or service to global average temperature increase of the atmosphere at a future point in time, typically at 100 years.

Both GWP and GTP are recommended emission metrics by the IPCC[6] and have been suggested as complementary CFs for quantification of climate change impacts of products and services by the LCA community.[9] However, none of them considers climate tipping mechanisms in the earth system.[9,10] It is challenging to capture the dependence of the impact of emissions on the emission timing in relation to the time of the tipping points. As tipping points represent critical levels of warming that should not be crossed, tipping-orientated GHG emission metrics cannot simply measure radiative forcing (or temperature) change over a fixed time horizon for a pulse emission emitted at an arbitrary time. Instead, they should quantify how much that change can contribute to crossing the tipping points and should assess that for multiple pulse

Received: May 7, 2020
Revised: January 27, 2021
Accepted: January 29, 2021
Published: February 5, 2021

emissions, i.e., emitted at different times. To do this, an approach based on quantification of the carrying capacity of the atmosphere to absorb the emission without crossing the tipping point is necessary.[11] In this perspective, the effects of an emission will depend on how much carrying capacity is depleted by the emission and, thus, on the proximity to tipping points. This is at odds with current impact assessment practice where carrying capacities and dependency of impacts on emission timing are not embedded in the CF.[11,12]

The metric developed by Jørgensen et al.,[13] the climate tipping potential (CTP), introduced both aspects while accounting for the Arctic summer sea-ice loss as tipping element. Here, the impact of 1 kg GHG emitted at a given year was expressed as the fraction of carrying (or remaining) capacity, i.e., the time-integrated increase in atmospheric CO_2-equivalent concentration that can still occur before Arctic summer sea-ice loss, depleted by the time-integrated change in CO_2-equivalent concentration caused by the emission. However, their metric only considers this one tipping point and thereby neglects several aspects that are required for a robust metric of climate tipping. First, it must consider emissions occurring after the tipping of a given element of the earth system as contributors to crossing other, subsequent tipping points.[13] Second, potential consequences of crossing a given tipping point on the acceleration tipping of other elements must be accounted for.[14] For instance, the reduction of sea ice albedo in the Arctic amplifies warming making the subsequent tipping point (e.g., Greenland ice sheet melting) occur faster than it would without tipping of the Arctic sea ice. Third, when taking multiple tipping points into account, sequence and timing of occurrence of individual climate tipping points depend on uncertain factors, like temperature thresholds triggering the tipping points,[2,15] and these uncertainties must be accounted for.

In this paper, we develop new climate tipping characterization factors (CF) for three major anthropogenic GHGs (carbon dioxide (CO_2), methane (CH_4), and nitrous oxide (N_2O)), which meet these requirements. We first select relevant tipping elements, present the conceptual framework, and develop a method for computing multiple climate tipping points potentials (MCTPs) at midpoint. We apply the new MCTPs to end-of-life GHG emission inventories for plastic polymers made from different feedstock and spanning a wide range of temporal evolutions of GHG emissions in their end-of-life. We also present practical implications of using the new CFs in LCA, where information about temporal evolution of GHG emissions might not be available or relevant. We argue that the new CFs are a useful supplement to (but not a substitute for) the currently used GWP and GTP CFs recommended by the IPCC.

METHODS

Selection of Climate Tipping Elements. We carried out a literature review to identify a broad list of potential tipping elements without considering potential differences in the formal definition of tipping point given by different authors (Table S1 in Supporting Information). From this broad list, 13 tipping points were selected for inclusion in the study based on a set of criteria that (1) define the tipping mechanism, (2) consider changes in atmospheric GHGs concentration as the potential triggers, and (3) consider modeling of the tipping points feasible when tipping thresholds can be expressed as global mean temperature. The selection criteria are presented in the Supporting Information. The selected tipping points are Arctic summer sea ice loss (AS), Greenland ice sheet melt (GI), West Antarctic ice sheet collapse (AI), Amazon rainforest dieback (AF), Boreal forest dieback (BF), El Niño-Southern Oscillation change in amplitude (EN), Permafrost loss (P), Arctic winter sea ice loss (AW), Atlantic thermohaline circulation shutoff (TC), North Atlantic subpolar gyre convection collapse (SG), Sahara/Sahel and West African monsoon shift (AM), Alpine glaciers loss (AG), and Coral reefs deterioration (CR) (Table S2).

Conceptual Framework. The method for calculating the climate tipping potential (CTP) for the Arctic summer sea-ice loss as tipping element proposed by Jørgensen et al.[13] was taken as a starting point. Their method is further developed to consider: (1) other selected tipping elements, (2) uncertainties of tipping points occurrence, and (3) the effect of crossing a tipping point on accelerating tipping of all subsequent tipping points. The new CFs are therefore referred to as multiple climate tipping points potentials (MCTP). Their main features are presented below.

First, the impact of a GHG emission represents time-integrated radiative forcing of 1 kg emission of a greenhouse gas i and is expressed as atmospheric CO_2-equivalent concentration (in ppm of CO_2e·yr·kg_i^{-1}). The integration is from the emission year to the year of tipping (rather than over a fixed time horizon like in the GWP).

Second, this impact is always given in relation to the remaining capacity of the atmosphere to absorb that impact without triggering the tipping point, also expressed in ppm of CO_2e·yr·kg_i^{-1} (rather than comparing impacts to that of a reference gas like CO_2 as in GWP). The resulting MCTP CFs therefore represent the fraction of remaining capacity taken up by the unit emission (which is expressed in parts per trillion of remaining capacity, ppt_{rc}·kg_i^{-1}). MCTPs are dynamic because both the impact and the remaining capacity to absorb the impact without triggering the tipping point depend on emission time.

Third, remaining capacities depend on background anthropogenic GHG emissions, as they ultimately determine when the tipping point is triggered, and furthermore, the impact of a GHG emission attributed to a product or service can be considered as part of this background. Although GHG emissions from an individual product system will never be large enough to cause a tipping, a large number of products that are produced, used, and disposed of in our society and their attributed (often very small) quantities of GHG emissions have a real potential to cause the tipping. Thus, application of MCTP CFs to single product systems that are modeled in LCA gives a meaningful estimate of the product's contribution to passing critical tipping points. This is in line with the attributional approach to LCA, which aims to represent a product system in isolation to quantify the impact that the product is "responsible for".[16] However, considering the effects from crossing a given tipping point on the reduction of the remaining carrying capacity for all subsequent tipping points could be seen as a marginal contribution that adds impact to the background pressure. This is more in line with the consequential approach to LCA, which aims to assess the environmental consequences of using a product or providing a service.

Finally, the aforementioned considerations imply that MCTP CFs are not applicable to assessments of large scale

https://dx.doi.org/10.1021/acs.est.0c02928
Environ. Sci. Technol. 2021, 55, 2800−2810

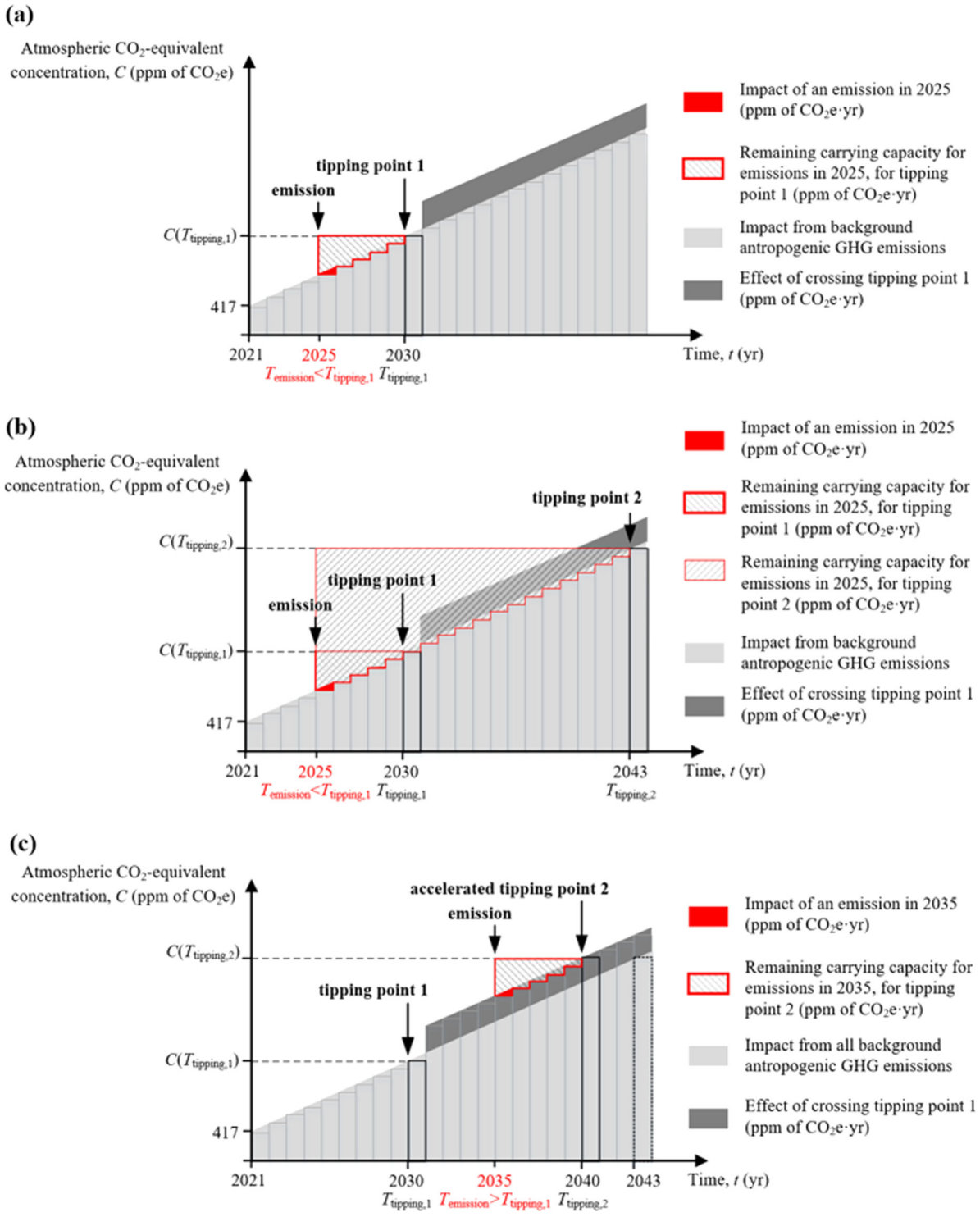

Figure 1. Conceptual illustration of MCTP calculation for a unit (1 kg) emission of GHG i that is part of anthropogenic background GHG emissions, in different years with either one (a) or two (b and c) tipping points. The horizontal time axis is divided in discrete time intervals of 1-year, as indicated with capital letters, and vertical bars represent annual CO_2-equivalents concentration increases. $T_{emission}$ indicates the emission year; $T_{tipping,1}$ and $T_{tipping,2}$ indicate the year of tipping of the first and second tipping point, respectively. Emissions occurring before the first tipping point (at $T_{emission} < T_{tipping,1}$) will contribute to crossing both tipping points (at $T_{tipping,1}$ and $T_{tipping,2}$). Emissions occurring after the first tipping point but before the second tipping point (at$T_{tipping,1} < T_{emission} < T_{tipping,2}$) will contribute to crossing the second tipping only. Crossing the first tipping point speeds up the occurrence of the second tipping point, in practice, reducing the carrying capacity of emissions at $T_{tipping,1} < T_{emission} < T_{tipping,2}$ for the second tipping point. Note that the effect of crossing the first tipping is irrelevant for part a because this case considers only one tipping point (as presented in Jørgensen et al.[13]) and is not considered in calculation of remaining carrying capacity for an emission occurring before the first tipping point.

systems, e.g., at country level, which have the potential to substantially influence background emission levels.

Figure 1 provides a conceptual illustration of the framework: starting from one tipping element (in practice, CTP of

https://dx.doi.org/10.1021/acs.est.0c02928
Environ. Sci. Technol. 2021, 55, 2800−2810

Jørgensen et al.[13]) (Figure 1a) through adding a second tipping point (Figure 1b) to considering effects from crossing the first tipping point on accelerating tipping of the second tipping point (Figure 1c). The figure is conceptual as (1) increase in atmospheric CO_2-equivalent concentration due to background anthropogenic emissions is assumed linear, (2) the impact of the emission (part of anthropogenic background emissions) is simplified using triangles, (3) the remaining capacity is also simplified using triangle-like shapes, and (4) the effect of crossing the first tipping point is assumed to be equally distributed over the years which follow. Yet, the figure allows us to illustrate the framework. Background production and consumption activities increase atmospheric CO_2-equivalent concentration so that the first tipping point is triggered in 2030. An emission before this tipping point, e.g., in 2025, contributes to the crossing of this tipping point as it consumes part of the carrying capacity that remains until the tipping point is triggered (Figure 1a). This is the principle of the original CTP-framework of Jørgensen et al.[13] Extension of their framework by considering another tipping element, here triggered in 2043, implies that an emission in 2025 now contributes to crossing of both tipping points as it also consumes part of the carrying capacity that remains until the second tipping point is triggered (Figure 1b). Finally, for an emission occurring after the first tipping point but before the second one, e.g., in 2035, one additional factor must be considered. Namely, crossing of the first tipping point in 2030 speeds up tipping of the second tipping point (from 2043 to 2040) because of the effect from the tipping of the first tipping point itself which adds to the background (Figure 1c). This accelerated tipping of the second tipping point reduces the remaining capacity for those emissions which occur after the first tipping point.

The same mechanisms apply if more tipping points are considered. Mathematical description of these mechanisms is detailed later.

Consideration of Time as a Variable. The MCTP framework requires that the time variable is used with different attributes. Specifically, we distinguish *time interval* (i.e., time step) where time is discrete as opposed to *point in time* where time is continuous. The *interval* is used when time indicates a portion (an interval) of time defined within two specific points in time. It is indicated with capital T. For instance, the emission year $T_{emission}$ = 2021 indicates an emission occurred any time between first January, 00:00 and 31st December, 23:59 of the year 2021. Intervals of 1 year were considered the most realistic level of resolution for time-differentiated inventories of emissions and thus for the calculation of MCTPs. *Points in time* were used when integration over time was necessary. Time in those cases is a continuous variable and is indicated with lowercase t. We also distinguish between *absolute time* as opposed to *relative time.* Time is generally absolute in our framework because MCTPs depend on the specific years in which tipping points are triggered (e.g., 2021, 2022, etc.). By contrast, whenever the dependent variable does not depend on the proximity to tipping point, then relative time is used (e.g., year 1, year 2, etc.). A summary of the symbols used to refer to the time variable, their meaning, and where they are used in the paper is presented in Table S7 in Supporting Information.

Calculation of Multiple Climate Tipping Points Potentials (MCTP). With a consideration of m tipping points, the multiple climate tipping points potential, $MCTP_i$, in [ppt_{rc}·kg_i^{-1}] (parts per trillion of remaining capacity taken up by a unit emission) of gas i emitted at year $T_{emission}$ is defined as the sum of the ratios between the *impact of the emission* (that is part of anthropogenic background emissions) and the corresponding remaining capacity for each of the m tipping points occurring after the emission year

$$MCTP_i(T_{emission}) = \sum_{j=1}^{m} \frac{I_{emission,i,j}(T_{emission})}{CAP_j(T_{emission})} \quad (1)$$

where j indicates the jth tipping point occurring after the emission year (in order of occurrence) and can take any value from 1 to m, which is the total number of exceeded tipping points; $I_{emission,i,j}$ is the *impact of the emission* (part of anthropogenic background emissions) of gas i with respect to the jth tipping point, CAP_j is the remaining capacity up to the jth tipping point, and the emission year $T_{emission}$ can be any year from 2021 (or the year when emissions are expected to start taking place) up to the year of the last tipping point. Defined in this way, the MCTP represents the total fraction of remaining capacity taken up by the unit emission and is expressed in parts per trillion of remaining capacity (ppt_{rc}·kg_i^{-1}). The $I_{emission,i,j}$ [ppm of CO_2e·yr·kg_i^{-1}] (where CO_2e is the CO_2-equivalent concentration) of gas i with respect to the jth tipping point is here defined as the absolute climate tipping potential (ACTP) of gas i in [$W{\cdot}m^{-2}{\cdot}yr{\cdot}kg_i^{-1}$] divided by the radiative efficiency (RE) of 1 ppm of CO_2 [$W{\cdot}m^{-2}$·ppm of CO_2^{-1}][13]

$$I_{emission,i,j}(T_{emission}) = \frac{ACTP_{i,j}(T_{emission})}{RE_{CO_2}} = \frac{\sum_{k=1}^{n} RF_i(T_{k-1})\cdot\Delta T}{RE_{CO_2}} \quad (2)$$

where the ACTP is equal to the radiative forcing of gas i (RF_i) integrated over time between the emission and the tipping. This integral is written using Riemann sum notation. In this notation, n is the number of time steps (dimensionless). Given that $\lim_{n\to\infty}(n\cdot\Delta T) = (T_{tipping,j} - T_{emission})$, the n is equal to the difference between the year of tipping $T_{tipping,j}$ (i.e., the year when the jth tipping point is exceeded) and the year of emission, $T_{emission}$, divided by the length of the time step, ΔT (eq 3). The ΔT is always equal to 1 year.

$$n = \frac{T_{tipping,j} - T_{emission}}{\Delta T} \quad (3)$$

Note that time is relative in the RF function because radiative forcing increase depends on the time that has elapsed from the emission, independently of the emission year. However, the ACTP and the resulting *impact of the emission* are emission-year specific because year of tipping is given. The RF_i is calculated as the product of the radiative efficiency of gas i (A_i) (which represents radiative forcing per unit mass increase in atmospheric abundance of gas i) and the impulse response function (IRF), which for most non-CO_2 GHGs is represented with a single exponential decay and for CO_2 with a sum of exponentials.[8] However, unlike in the GWP approach, where radiative forcing of gas i is divided by the radiative forcing of the reference gas (CO_2), the radiative forcing of gas i is divided here by the radiative efficiency of CO_2, the RE_{CO_2}. This makes the unit of the *impact of the emission* consistent with the unit of remaining capacity (both given in ppm of

https://dx.doi.org/10.1021/acs.est.0c02928
Environ. Sci. Technol. 2021, 55, 2800−2810

CO_2e·yr). Details of calculations of the impact are presented in Supporting Information.

The CAP_j [ppm of CO_2e·yr] represents the increase in atmospheric CO_2-equivalent concentration that can still take place before reaching the concentration level (in ppm of CO_2e) that will trigger the tipping. It is emission-year specific as it depends on CO_2-equivalent concentration from background anthropogenic emissions. The remaining capacity is reduced when the emission year approaches the year of tipping due to the effect of crossing any preceding tipping points, C_{tip} (expressed in terms of CO_2-equivalent concentration increase). This effect reduces the CO_2-equivalent concentration increase that can still occur before reaching the year of tipping of subsequent tipping points thus accelerating their tipping. Equation 4 shows the calculation of the remaining capacity using Riemann sum notation for 1-year time steps

$$CAP_j(T_{emission}) = C(T_{tipping,j})\cdot(T_{tipping,j} - T_{emission}) - \sum_{k=1}^{n} [C(T_{k-1}) + C_{tip}(T_{k-1})]\cdot\Delta T \quad (4)$$

where $C(T_{tipping,j})$ is the atmospheric CO_2-equivalent concentration at the year of tipping $T_{tipping,j}$, $C(T)$ is the CO_2-equivalent concentration from background emissions at time T, and $C_{tip}(T)$ is the change in CO_2-equivalent concentration at time T caused by all the tipping points that occurred before $T_{emission}$ (all terms expressed in ppm of CO_2e). The $C_{tip}(T)$ is obtained from radiative forcing (RF) change induced by passing each specific tipping event (see Section S1.3.1 of Supporting Information). Time is absolute in eq 4 because both anthropogenic background emissions and effect of the tipping depend on the specific year. To avoid the capacity to become infinitely small and thus returning high peaks in MCTP, a cutoff of 6 [ppm of CO_2e·yr] was applied by taking the annual variability of atmospheric CO_2 concentration as a proxy for the uncertainties in measuring the atmospheric capacity (see Supporting Information).

Our representation of MCTP as a CF is somewhat different from the one that is typically used in LCIA. CFs typically represent either marginal or average "impact due to a unit emission".[16−19] The GWPs are derived in a marginal way,[16] and this is also the way the ACTP underlying $I_{emission,i,j}$ in numerator of eq 1 is calculated (as in the GWPs, it is derived through radiative forcing per unit mass increase in atmospheric abundance of a given gas; see eq 2 and S1). Yet, the resulting impact $I_{emission,i,j}$ is related to the remaining carrying capacity, which depends on the background level, which in turn follows RCP pathway projections that are not influenced by the system being assessed in the LCA. This suggests that the resulting MCTP CFs are more in line with the average approach to calculating characterization factors (which could be supported for this type of impact owing to assumption of additivity of impacts of GHG emissions[20]). Consideration of carrying capacity in the CF is not usual but has been discussed and tested previously.[21,22] Bjørn A.[23] showed how carrying capacity can be integrated into characterization factors for terrestrial acidification.

The framework presented above was used to compute the MCTP of the three main anthropogenic GHGs, CO_2, CH_4, and N_2O, considering the selected tipping elements, in 10000 Monte Carlo simulations. Each simulation represents a possible sample scenario of triggered tipping points (i.e., different timing and order of occurrence) based on the propagation of current uncertainties in tipping occurrence. An average (geometric mean) MCTP was then calculated. We observe that iterations fail whenever tipping points are triggered in close proximity to each other (either in the same year or in consecutive years) as no remaining capacity can be calculated. This is taken into account by adjusting the number of total iteration runs so that failed iterations are excluded while the total number of runs is ∼10000. Implications of this model limitation on the MCTP will be discussed.

Choice of Atmospheric GHG Concentration Development Pathway. Both the determination of the years of tipping and the evolution of the remaining capacity over time depend on the development of atmospheric GHG concentrations, expressed in CO_2-equivalents. Here, the Representative Concentration Pathways (RCPs) and their extensions up to year 2500 are used.[24,25] The medium stabilization pathway RCP6 (total radiative forcing stabilized at 6 Wm·$^{-2}$ after 2100) is chosen as baseline, assuming that even though current emission trajectories are closer to RCP8.5 projections,[26] ongoing mitigation efforts will prevent a continuous increase and will more likely lead to a peak-and-stabilization pathway as projected in RCP6. The MCTPs were also calculated for RCP8.5 (rising radiative forcing to 8.5 Wm·$^{-2}$ after 2100) and RCP4.5 (stabilization at 4.5 Wm·$^{-2}$ after 2100), selected as potentially worst- and best-case (realistic) pathways, respectively. The low emission scenario RCP2.6 is excluded as the massive mitigation efforts required are considered mostly unfeasible.[26,27] The choice of RCP pathway influences which tipping points are triggered in each simulation as it depends on whether the threshold temperature of a specific tipping element is reached under the RCP pathway.

Determination of Tipping Time. Accurate predictions of the climate conditions triggering a tipping point and the time of occurrence are uncertain.[3] On the basis of available estimates of potential thresholds levels (Table S1), we assigned one possible range of temperature thresholds to each selected tipping element (Table S2). Uncertainties in the actual temperature threshold level were accounted for by assigning a triangular probability distribution function to the range of potential threshold levels; $T(a,b,c)$, where a and b are the lower and upper limits of the range, respectively, and the most likely value c is assumed to be the central value of the assigned range. Triangular distribution was chosen because actual distributions were unknown and could not be generated with the limited data available.

The CO_2-equivalent concentration that stabilizes the climate at a given temperature threshold and the year of tipping were obtained by the combination of data on temperature and GHG concentration equivalents development over time, according to the chosen RCP pathway. The data are retrieved with the climate model MAGICC6 (Model for the Assessment of Greenhouse Gas Induced Climate Change, v.6), which is a default model to harmonize projections of RCP and Extended Concentration Pathways (ECP).[25,28]

Calculation of Effects from Crossing Climate Tipping Points (C_{tip}). Modeling of the possible consequences from passing a tipping point is constrained by the availability of quantitative estimates of the total magnitude of such effects, which are rather scarce in the scientific literature. We considered available estimates of the potential change in RF induced by tipping suggested in previous studies (Table S6),

https://dx.doi.org/10.1021/acs.est.0c02928
Environ. Sci. Technol. 2021, 55, 2800−2810

and to allow for their quantification in relation to the remaining capacity, we converted these to the increase in equivalents of GHG concentrations (ppm of CO_2e) that would lead to the same RF change. In some cases, the effect from tipping could not be modeled due to either lack of data (Atlantic thermohaline circulation shutoff, North Atlantic subpolar gyre convection collapse, Sahara/Sahel and West African monsoon shift, Alpine glaciers) or lack of consequences on the climate from the tipping point (coral reefs) (see Supporting Information). For Arctic summer and winter sea-ice loss, the RF change is due to reduced sea-ice albedo and conversion to annual concentration increase was done using the radiative efficiency of CO_2 per 1 ppm. This effect was assumed to unfold completely from the year after tipping and to remain constant over the years, as the evolution of radiative forcing changes after tipping was unknown. For the other six tipping points, i.e., Greenland ice sheet melt, West Antarctic ice sheet collapse, El Niño-Southern Oscillation change in amplitude, permafrost loss, Amazon rainforest and Boreal forest dieback, the RF change derives from emissions of carbon estimated to occur after tipping (Table S6). Here, C_{tip} was calculated by adapting the dynamic approach of Levasseur et al.,[29] originally developed for calculating time-dependent RF impacts of GHG emissions (that is, dynamic global warming potentials), to obtain time-dependent (dynamic) yearly equivalents of GHGs concentration increase due to the carbon emissions. The total carbon emissions, considered to be either CO_2 or methane emissions, depending on the tipping element, were assumed to be equally distributed over the transition period of the tipping event (see Table S6 in Supporting Information), obtaining a constant temporal profile of emissions. An exception is for El Niño-Southern Oscillation change in amplitude for which the release of carbon is considered basically permanent.[4] The effect of these emissions was then calculated considering the residence time of the two gases in the atmosphere. The result provides the equivalent increase in GHG concentrations at any time T after tipping, caused by the emissions released at T and the nondecayed fraction of emissions that occurred before T since the tipping year. This approach does not account for the gradual changes that in reality occur before a critical point is reached (e.g., albedo changes from melting sea ice at current temperature levels) and may underestimate the actual effects from tipping. However, it was the most feasible modeling option considering model complexity constraints and lack of estimates on the gradual changes expected before reaching some of the considered tipping points. Details of these calculations are presented in Section S1.3.1 of Supporting Information.

Illustrative Application. The CFs proposed here depend on the year of emission, hence for each GHG, a set of year-specific MCTPs is provided and this should be used in combination with a time-differentiated inventory specifying GHG emissions in each year. The resulting impact score is calculated by summing the product of the emitted amount of gas i at year $T_{emission}$ with the corresponding MCTP factor at $T_{emission}$ for each GHG i and each emission year $T_{emission}$

$$IS_{MCTP} = \sum_{i} \sum_{T_{emission}=2021}^{T_{tipping,j_{last}}} m_i(T_{emission}) \cdot MCTP_i(T_{emission}) \quad (5)$$

where IS_{MCTP} is the MCTP impact score, $T_{tipping,j_{last}}$ is the last possible year when a tipping point can be triggered across 10000 model runs, j_{last} is the last triggered tipping point across 10000 model runs, $m_i(T_{emission})$ is the mass of GHG i emitted at year $T_{emission}$, and $MCTP_i(T_{emission})$ is the corresponding MCTP for gas i and emission year $T_{emission}$. The double summation indicates that the product $(m_i(T_{emission}) \cdot MCTP_i(T_{emission}))$ is first summed over time, starting from the first emission of GHG i released by the assessed product (assumed to be year 2021 in eq 5) up to the year when MCTPs are relevant ($T_{tipping,j_{last}}$), and then summed over each GHG i.

We apply the MCTPs calculated for the RCP6 scenario to CO_2 and CH_4 emission profiles (over 100 years) from incineration and landfilling of 1 kg of fossil-based (polycaprolactone (PCL), polybutylene succinate (PBS), polystyrene (PS)) and biobased (poly)lactic acid (PLA)) biodegradable polymers. These materials are selected as they degrade over different timespans when landfilled. Six landfilling scenarios are considered with four representing a possible range of degradation rate constants (corresponding to fast, medium, slow, and very slow first order[30] degradation kinetics under anaerobic conditions) and two accounting for delays in GHG emissions for a material with fast kinetics (20 and 50 years delay) as found for different fossil- and biobased plastic types.[30−33] For each scenario, the assumed carbon content of the degrading material is 0.5 kg C/kg plastic (stoichiometric calculation from a hypothetical polymer with 3 carbon atoms) of which 100% is released as CO_2 in the incineration scenario, whereas 71% is emitted as CO_2 and 29% as methane in the landfilling scenarios.[33] Note that only emissions stemming from the carbon contained in the plastic are considered. By multiplying the yearly emitted amount with the corresponding average MCTPs per unit emission (under RCP6), we used eq 5 to calculate total tipping impacts corresponding to degradation of 1 kg of plastic. For comparison, we also compute impact scores using the complementary CFs GWP20,[6] GWP100,[6] $GWP100_{ILCD}$, i.e., including credits for temporary carbon storage using the method in the ILCD Handbook,[34] dynamic GWP100,[29,35] and GTP100.[8,10] While GWP100 treats emissions over 100 years as a pulse emission in the first year, dynamic GWP100 expresses the time-dependent contribution of emissions to radiative forcing change over 100 years, accounting for the actual emission timing. $GWP100_{ILCD}$ includes credits for temporary carbon storage to account for the storage due to delayed or incomplete degradation of the plastic materials over 100 years. In consistency with recommended practice,[12] all GWP CFs are inclusive of climate-carbon cycle feedbacks. Methods for calculating impact scores using all these CFs are summarized in Table S9 in Supporting Information.

RESULTS

Multiple Climate Tipping Potentials. Results of two successful Monte Carlo simulations show that the number and type of tipping points actually triggered depends on the probability that the threshold temperature picked in the simulation is within the temperature increase projected under the chosen pathway (Figure 2a,b). They also show that MCTPs are particularly sensitive to the proximity of an emission year to the year of tipping. The MCTP can increase by up to a factor of 6 compared to the MCTP for an emission in year 2021 when emission year approaches the year of tipping, and it drops consistently after the tipping point is

https://dx.doi.org/10.1021/acs.est.0c02928
Environ. Sci. Technol. 2021, 55, 2800−2810

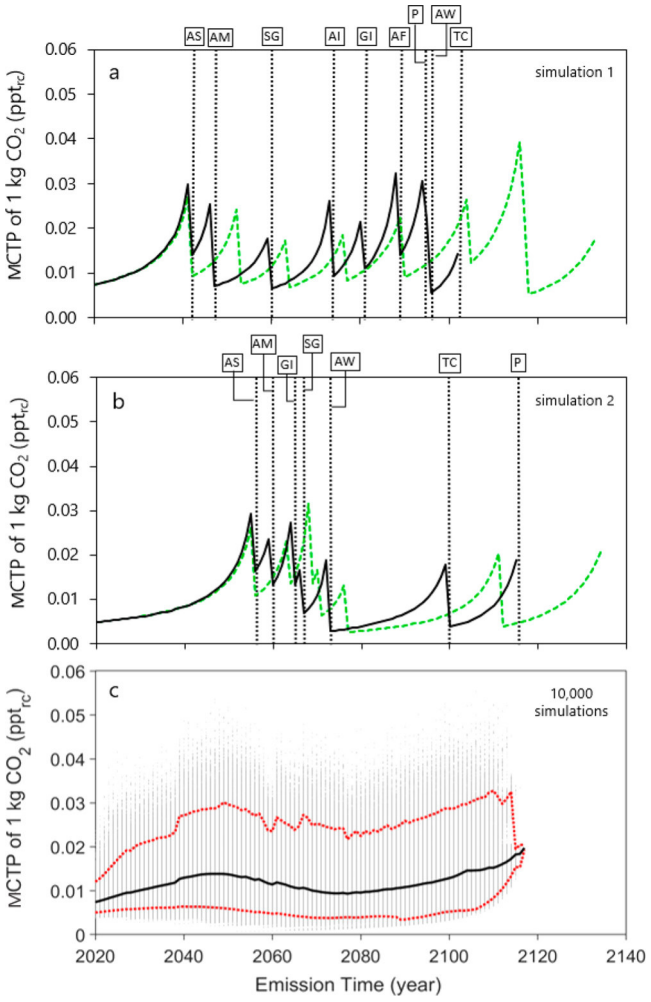

Figure 2. Emission-year specific multiple climate tipping point potentials (MCTP) per emission of 1 kg CO_2 under RCP6. (a, b) MCTPs from two illustrative model simulation runs (solid line). Vertical dotted lines indicate occurrence of tipping points (Table S8). Green dashed curves are the same simulations computed without considering the effect from the tipping (tipping occurrence not shown in this case). AS = Arctic summer sea ice loss, AM = West African monsoon shift, SG = North Atlantic subpolar gyre convection collapse, AI = West Antarctic ice sheet collapse, GI = Greenland ice sheet melt, AF = Amazon rainforest dieback, *P* = Permafrost loss, AW = Arctic winter sea ice loss, TC = Atlantic thermohaline circulation shutoff. (c) MCTP results for 10000 model simulations (gray dots), their geometric mean (solid line) and uncertainty ranges (5th and 95th percentiles of yearly results, red dotted lines).

crossed, causing discontinuities in the MCTP curve. The steep increases in the MCTP are caused by fast reduction in the remaining atmospheric capacity assigned to these tipping points when emission years approach respective years of tipping (see Figure S3 in Supporting Information). The drop in the MCTP after crossing a given tipping point is caused by capacities assigned to the subsequent tipping always being significantly larger when compared to the remaining capacity assigned to the preceding tipping event. Accounting for direct effects from crossing tipping points in these two simulations reduces the remaining capacity from 10 to 99% (depending on the emission year) when compared to model results without considering the effect from the tipping on remaining capacity up to the next tipping point(s). This accelerates the occurrence of the subsequent tipping points by 3 to 31 years.

The tendency of MCTP to peak with the proximity to a tipping point is masked by the large uncertainties around the year of tipping, which influence the number and sequence of tipping points and make individual tipping points overlap. Average (geometric mean) MCTP derived from ~10000 Monte Carlo simulations varies from 0.0074 to 0.020 ppt_{rc} per 1 kg of CO_2 emission (Figure 2c). In 90% of the iterations, MCTPs ranged from 0.0034 to 0.033 ppt_{rc} per 1 kg of CO_2 emission across all emission years. Yet, there is a relatively high probability of several tipping points occurring between 2040 and 2060, resulting in a peak of average MCTPs around 2050 with almost a doubling of the MCTP magnitude (average 0.014 ppt_{rc}) in comparison to emissions occurring in 2021 (average 0.0074 ppt_{rc}). Average MCTPs of CH_4 and N_2O follow the same trends as observed for CO_2 in Figure 2c but are on average 83 and 273 times higher, respectively, when compared to CO_2 (Figure S4). The impact of a unit emission of CH_4 is higher than that of CO_2 in the MCTP approach when compared to GWP100, because the time integrations in ACTP are over shorter time periods compared to the 100 years' time horizon of GWP, and with shorter time horizons, the impacts of short-lived gases like CH_4 become larger.

Consideration of direct effects from the tipping increases the average MCTPs by up to 37% when compared to the average MCTP computed without considering the effect from the tipping (with greater increases for emissions occurring later in time). This corresponds to the last tipping point occurring, on average, 17 years earlier (Figure S5).

The MCTPs calculated for different RCP pathways follow different trends (Figure 3). They are larger when assuming a low background concentration pathway (RCP4.5) and become progressively smaller for higher concentration paths RCP6 and 8.5. The MCTPs increase until 2035 in all pathways, but then they fluctuate over the middle in RCP6, increase in RCP4.5, and follow a downward trend in RCP8.5. The number of tipping points that can be triggered also varies between RCP scenarios, depending on whether threshold temperatures are reached (Table S2). In the high emissions pathway RCP8.5, all the 13 elements can have their tipping points crossed. In RCP6, the permafrost loss and Arctic winter sea ice loss are not triggered, while under RCP4.5, additionally Boreal forest dieback, El Niño-Southern Oscillation change in amplitude, and Atlantic thermohaline circulation shutoff are not triggered. These differences in the number of tipping points determine the time horizon for which MCTPs are relevant (until 2085, 2115, and 2210 in the RCP4.5, RCP6, and RCP8.5 scenarios, respectively).

Example of Degradation of Plastic Polymers. We find that using new MCTPs leads to additional insights when compared to those gained from using other metrics (Table 1). Impact scores in the MCTP approach increase with decreasing degradation rates (scenarios 2−4) because there is higher probability that a significant portion of emissions is released in close proximity to tipping points, where MCTPs are the largest (Figure S6). By contrast, impact scores generally decrease with decreasing degradation rate in the GWP-based and GTP100 approaches owing to (1) decreasing emissions released within the 20 (GWP20) and 100 years (GWP100, GTP100) time horizons, (2) increasing benefits from temporary carbon storage ($GWP100_{ILCD}$), and (3) delayed emissions and smaller values of their matching dynamic GWP100. With MCTP, a 20-

https://dx.doi.org/10.1021/acs.est.0c02928
Environ. Sci. Technol. 2021, 55, 2800−2810

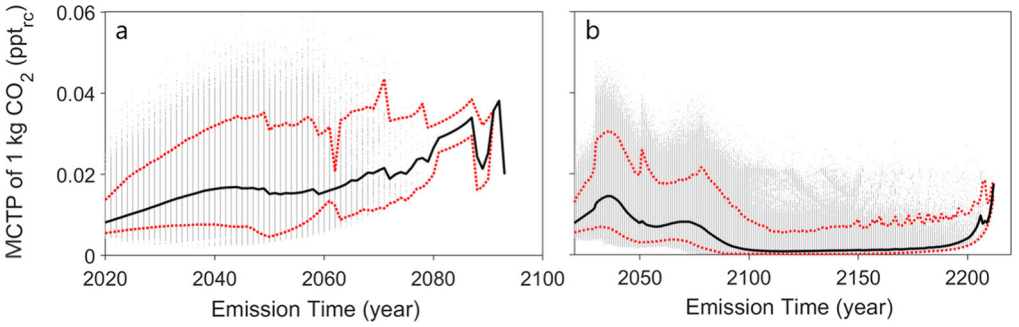

Figure 3. Emission-year specific multiple climate tipping points potentials (MCTP) of 1 kg of CO_2 under RCP4.5 (a) and RCP 8.5 (b) scenarios. MCTPs for 10000 model simulations (gray dots), their geometric mean (solid line), and uncertainty ranges (5th and 95th percentiles, red dotted lines). Notice the different scale of the *x*-axes.

Table 1. Total Impact Scores for Different End-of-Life Scenarios of Plastic Polymers Calculated Using GWP20, GWP100, $GWP100_{ILCD}$, Dynamic GWP100, GTP100, and New MCTPs[h]

End-of-life degradation scenario	GWP20 (kg CO_2eq/kg plastic)	GWP100 (kg CO_2eq/kg plastic)	$GWP100_{ILCD}$ (kg CO_2eq/kg plastic)	Dynamic GWP100 (kg CO_2eq/kg plastic)	GTP100 (kg CO_2eq/kg plastic)	MCTP, under RCP6 (ppt_{rc}/kg plastic)
1. Incineration[a]	1.8	1.8	1.8	1.8	1.8	0.014
Plastic degradation rate[b]						
2. Fast[c]	18	8.3	8.2	4.7	3.8	0.089
3. Medium[d]	14	8.3	7.4	4.6	3.8	0.14
4. Slow[e]	6.4	7.3	5.5	3.8	3.4	0.16
5. Very slow[f]	0.036	0.078	0.048	0.052	0.034	0.0020
Delayed degradation[g]						
6. After 20 years (fast rate)	0	8.3	6.9	4.5	3.8	0.21
7. After 50 years (fast rate)	0	8.3	5.1	4.1	3.8	0.16

[a]Incineration of fossil-based plastic where all carbon is emitted as CO_2 in the first year. [b]Degradation under anaerobic conditions, resulting in release of methane. [c]90% degradation of polycaprolactone (PCL) in 2 years.[31] [d]90% degradation of polybutylene succinate (PBS) in 31 years.[32] [e]90% degradation of polystyrene (PS) in 105 years.[30] [f]1% degradation of biobased PLA in 100 years.[33] [g]Potential short (20 years) and long (50 years) lag phase in degradation of PCL based on ref 33. [h]Ranking between scenarios 1−7 is illustrated within each column with different colors. Red shading indicates the highest impact scores and green the lowest impact scores. The $GWP100_{ILCD}$ includes credits for the temporary carbon storage of delayed or incomplete degradation of the material over 100 years calculated using the ILCD approach.[34]

and 50-year lag phase of degradation of the polymers are seen as worse and second worse scenarios, respectively, because of proximity of emissions to tipping points, whereas with GWP100 and GTP100, which are not able to capture differences in emission timing, impact scores are the same as without a lag phase (scenario 2). The MCTP results for these two scenarios are also different from GWP20, which does not assign any burden to emissions occurring after the 20 year time horizon. For very slow degradation kinetics, impact scores are almost independent of the type of metric chosen. This is because the vast majority of emissions in this slow degradation scenario occurs beyond the time frames for which MCTP and their complementary GWPs are considered relevant. Incineration is seen as the second best option with all other metrics, because no methane emissions occur and, for MCTP, also because of small CF values for emissions of CO_2 in year 2021.

Ranking of these different end-of-life scenarios was not very sensitive to the RCP pathway for which MCTPs were computed (Table S10); however, slight variations reflect the different contribution to tipping that emissions have in the three RCPs. In particular, under RCP4.5, the largest contribution is observed after 2060; therefore, a polymer with 50 years lag phase, emitting mostly around 2070, performs worse. In terms of magnitude, impact scores with RCP4.5 are larger for each end-of-life scenario, as the corresponding MCTP factors are larger.

DISCUSSION

Importance of GHGs Development Pathway. We find that the magnitude of the MCTPs is larger under RCP4.5 and lower under RCP8.5. This somewhat counterintuitive finding can be explained by two factors. First, the MCTP is a metric expressing midpoint impacts and, as such, it does not consider the severity of the damage on ecosystems or humans caused by crossing tipping points. These damages are expected to be larger for the RCP8.5 path when compared to those of the two other pathways. Thus, the impact expressed by our midpoint CFs should only be interpreted as the contribution of an emission that is part of the background to crossing tipping points and not as the overall damage caused by the emission or

https://dx.doi.org/10.1021/acs.est.0c02928
Environ. Sci. Technol. 2021, 55, 2800−2810

the damage caused by the tipping itself. Second, climate responds differently to the same increase in GHG concentrations in the three RCPs: for example, to reach a tipping threshold of 2 °C under RCP8.5, the GHG concentrations should rise to about 574 ppm of CO_2e, whereas 541 ppm of CO_2e are already sufficient according to RCP4.5 projections (Figure S1). This is because the slow heat uptake of the oceans creates a delay in the response of the atmospheric temperature to an increase in CO_2 concentration,[36] and this delay depends on the different rate of CO_2 increase projected in each RCP pathway. In RCP8.5, CO_2 concentrations increase rapidly, generating a larger lag in the climate response compared to RCP4.5. Therefore, RCP8.5 reaches 2 °C at higher concentrations, whereas in RCP4.5, the same temperature corresponds to lower concentration levels. This means that the contribution of an emission to crossing tipping points is proportionally larger under RCP4.5 because tipping points are triggered at lower concentrations when compared to RCP8.5 or RCP6. Consequently, for the same emission year, MCTPs are larger for RCP4.5 than for the two other pathways.

Differences in the temporal evolution of MCTPs observed between the RCP pathways are the result of a combination of several additional factors and it is not possible to determine one dominant driver. One factor is the different rate of projected GHGs concentration increase across the RCPs. In RCP8.5, GHGs concentration increases fast and, due to this, differences in concentration between consecutive years became larger over time (remaining capacity depends on the magnitude of the difference). In addition, tipping points are triggered at higher concentration levels, as explained above. This results in numerically larger remaining capacities for emissions in, e.g., 2080 than emissions in 2040 and explains why MCTP decreases over time. For RCP4.5, the opposite is true: MCTP increases over time because of relatively small differences in GHGs concentration between consecutive years (especially when the concentration starts to level off) and because tipping points are triggered at lower concentrations. Other factors to consider are the simultaneous dependency on evolution of *impacts of the emission* (as MCTPs are based on ratios between *impacts of the emission* and remaining capacities), the different number of tipping points that can be triggered in each RCP pathway, and the possibility, in RCP8.5, that tipping points occur at very high concentrations and very late in time (as opposed to no more tipping points beyond 2100 in RCP4.5).

Uncertainties. The major source of uncertainty in the MCTP CFs is that they do not consider interactions between the tipping elements.[4] Similarly, the MCTPs do not consider situations where tipping points are predicted to occur so close to each other that the remaining capacity is fully consumed by the preceding tipping points. Our results show that the probability that crossing a tipping point causes tipping of another (for at least one pair of tipping elements), even without considering other interactions,[37] is equal to 92% for the RCP6 scenario but is somewhat smaller for RCP4.5 and RCP8.5 (79 and 53%, respectively). This is consistent with earlier studies suggesting that the passing of some tipping points increases the likelihood of other tipping points due to positive feedbacks from the tipping.[38,4] The implication of this model limitation is that the time horizon for which MCTPs are relevant can be shorter. Another implication is that our MCTPs can be underestimated, particularly those occurring later where uncertainties about temperatures triggering the tipping are larger. The combined effect of more tipping points triggered at once would indeed reduce the remaining capacity to the next tipping even further, resulting in higher MCTPs. This is particularly the case for the RCP6 pathway, where the chances of one or more tipping points triggered at the same time is the highest. However, *impacts of the emission* will simultaneously decrease, as tipping points approach, and whether this results in an increase in MCTP will thus depend on the magnitude of reduction of the *impact of the emission* in relation to the reduction in remaining capacity.

Implications for Life Cycle Assessment. We offer a new method that considers multiple climate tipping points in the quantification of the potential contribution of products to climate change impacts. As no other metric considers the contribution of emissions to deplete the remaining capacity up to multiple tipping points and the variability of this contribution based on emission timing, the new method represents a new life cycle impact category. This new impact category should be seen as being complementary to, but not a substitute for, global warming and global temperature change categories. A ranking of the three well-mixed GHGs (CO_2, CH_4, and N_2O), in terms of their average MCTP, is comparable to the ranking of their GWP20s and ranges from 1:51:238 to 1:107:299 (RCP6), depending on emission year, in comparison to the constant ranking of 1:86:268[10] for the GWP20. This stresses the need to consider short-term climate impacts, as in both CFs, the radiative forcing is integrated over shorter time horizons (through the ACTP and AGWP), resulting in larger impacts assigned to short-lived gases like methane. Despite this similarity, the added value of the MCTP is that it captures those emissions and short-term impacts occurring beyond the 20-year time.

We showed that the use of MCTPs offers new insights when applied to temporarily differentiated GHG emission inventories. The best performance, from the climate tipping perspective, is achieved when emissions from the product occur when their contribution to crossing tipping points is the lowest rather than when these emissions are just delayed. Indeed, there is a high probability of several tipping points occurring from ca. 2040 to 2060, where MCTPs are the largest. An accounting for the uncertainties in the triggering of tipping points eventually results in a more robust, but perhaps less straightforward, assessment of climate tipping impacts from products. These uncertainties are currently so large that individual tipping points are not clearly discernible. Nevertheless, such large uncertainties should not prevent the use of MCTP because we demonstrated that MCTP still allows the capture of differences in performance of products with different temporal emission profiles.

We recall that the availability of time differentiated emission inventories of the assessed products is necessary for a meaningful use of the set of emission-year-specific MCTPs provided here (Supporting Information). The main implications for life cycle inventory (LCI) modelers is the need to focus on modeling and the reporting of emission inventories in temporarily disaggregated forms. The main implication for LCA software developers is the need to develop modules that can calculate impact scores using temporarily disaggregated inventories and time-dependent characterization factors. The same challenges are still relevant for dynamic methods, including the dynamic GWP approach.[29] We expect that potential take up of climate tipping as an impact category in LCA will make it attractive to increase the availability of

https://dx.doi.org/10.1021/acs.est.0c02928
Environ. Sci. Technol. 2021, 55, 2800−2810

temporarily differentiated emission inventories and their handling in LCA software. Until then, dynamic approaches, including our MCTP, have to be used offline.

The reader should note, however, that the iterative nature of LCA allows using our MCTP factors even if a full time-differentiated inventory is not available for all processes in a given life cycle. In this case, the ideal would be to identify processes where time-differentiation of emissions is relevant and is expected to really matter for the LCA results (such as end-of-life processes, biomass growth, or deforestation) and obtain a time-differentiated inventory for these processes only. This can be done with a sensitivity analysis. The MCTP impact score for these processes can then be calculated offline using eq 5. The impact score for all the remaining processes not associated with a time-differentiated inventory, or for those processes which do not matter for the LCA results (small contribution to total impact), can be calculated by multiplying the total amount of CO_2, CH_4, and N_2O emissions from these processes by the corresponding MCTP factor relative to the year when their emission is expected to take place. The sum of the two impact scores returns the final MCTP results.

The new metric is expected to be particularly valuable in the life cycle assessments of biodegradable plastics, deteriorating wooden products, or engineered chars used for temporary carbon storage.[35,39] We recommend the presenting of results for all three considered RCP scenarios to show if, and how, the choice of future uncertain emission pathways could influence conclusions of the study of interest. Our MCTPs are expected to add less value in the comparative LCA context when emissions occur all at once, such as the incineration scenario in our case study, or when there are large differences in the emitted amount of GHGs (e.g., very slow degradation scenario). Further, although emissions do not influence the background emission path, the MCTPs are not directly applicable in the assessment of large-scale systems, like economic sectors or countries.[13] Other midpoint CFs, like GWP and GTPs, are better suited for this purpose.

The MCTP is proposed as a method for climate change impacts at the midpoint level; therefore, the interest here is to cover only climate change impacts at the midpoint level. If crossing a tipping point leads to loss of species (directly by, e.g., loss of habitat when ice melts, or indirectly via temperature increase), then this should be accounted for at the damage level.

■ ASSOCIATED CONTENT

Supporting Information

The Supporting Information is available free of charge at https://pubs.acs.org/doi/10.1021/acs.est.0c02928.

Emission-year specific MCTP values (XLSX)

Methods and results (PDF)

■ AUTHOR INFORMATION

Corresponding Author

Serena Fabbri − *Quantitative Sustainability Assessment Group, Department of Technology, Management and Economics, Technical University of Denmark, Lyngby, Denmark;* orcid.org/0000-0001-8073-5469; Email: serf@dtu.dk

Authors

Michael Z. Hauschild − *Quantitative Sustainability Assessment Group, Department of Technology, Management and Economics, Technical University of Denmark, Lyngby, Denmark*

Timothy M. Lenton − *Global Systems Institute, University of Exeter, Exeter EX4 4QE, U.K.*

Mikołaj Owsianiak − *Quantitative Sustainability Assessment Group, Department of Technology, Management and Economics, Technical University of Denmark, Lyngby, Denmark;* orcid.org/0000-0002-6834-6249

Complete contact information is available at: https://pubs.acs.org/10.1021/acs.est.0c02928

Notes

The authors declare no competing financial interest.

■ ACKNOWLEDGMENTS

We acknowledge the financial support given by the European Commission under Horizon 2020; H2020-BBI-JTI-2016: BioBarr, grant agreement 745586. We thank Cedric Wannaz (Eurisko Research; MathWorks) for his assistance with the mathematical notation. We thank Reinout Heijungs for the strong support and valuable suggestions for improving the paper.

■ REFERENCES

(1) Lenton, T. M.; Rockstrom, J.; Gaffney, O.; Rahmstorf, S.; Richardson, K.; Steffen, W.; Schellnhuber, H. J. Too Risky To Bet Against. *Nature* **2019**, *575* (7784), 592−595.

(2) Lenton, T. M.; Held, H.; Kriegler, E.; Hall, J. W.; Lucht, W.; Rahmstorf, S.; Schellnhuber, H. J. Tipping Elements in the Earth's Climate System. *Proc. Natl. Acad. Sci. U. S. A.* **2008**, *105* (6), 1786−1793.

(3) Lontzek, T. S.; Cai, Y.; Judd, K. L.; Lenton, T. M. Stochastic Integrated Assessment of Climate Tipping Points Indicates the Need for Strict Climate Policy. *Nat. Clim. Change* **2015**, *5* (May), 441−444.

(4) Cai, Y.; Lenton, T. M.; Lontzek, T. S. Risk of Multiple Interacting Tipping Points Should Encourage Rapid CO2emission Reduction. *Nat. Clim. Change* **2016**, *6* (5), 520−525.

(5) Owsianiak, M.; Bjørn, A.; Laurent, A.; Molin, C.; Ryberg, M. W. LCA Applications. In *Life Cycle Assessment: Theory and Practice*; Hauschild, M. Z., Rosenbaum, R. K., Olsen, S. I., Eds.; Springer International Publishing, 2018; pp 31−41. DOI: 10.1007/978-3-319-56475−3.

(6) Forster, P.; Ramaswamy, V.; Artaxo, P.; Berntsen, T.; Betts, R.; Fahey, D. W.; Haywood, J.; Lean, J.; Lowe, D. C.; Myhre, G.; Nganga, J.; Prinn, R. G., Raga, M. S., R. V. D Changes in Atmospheric Constituents and in Radiative Forcing. In *Climate Change 2007: The Physical Science Basic. Contribution of Working Group I to the Fourth Assessment Report of the Intergovernmental Panel on Climate Change*. Cambridge University Press; Solomon, S., Qin, D., Manning, M., Chen, Z., Marquis, M., Averyt, K. B., Tignor, M., Miller, H. L., Eds.; Cambridge University Press, Cambridge, United Kingdom and New York, NY, USA., 2007.

(7) Laurent, A.; Owsianiak, M. Potentials and Limitations of Footprints for Gauging Environmental Sustainability. *Curr. Opin. Environ. Sustain.* **2017**, *25*, 20−27.

(8) Shine, K. P.; Fuglestvedt, J. S.; Hailemariam, K.; Stuber, N. Alternatives to the Global Warming Potential for Comparing Climate Impacts of Emissions of Greenhouse Gases. *Clim. Change* **2005**, *68*, 281−302.

(9) Jolliet, O.; Anton, A.; Boulay, A.-M.; Cherubini, F.; Fantke, P.; Levasseur, A.; McKone, T. E.; Michelsen, O.; Mila i Canals, L.; Motoshita, M.; Pfister, S.; Verones, F.; Vigon, B.; Frischknecht, R. Global Guidance on Environmental Life Cycle Impact Assessment

Indicators: Impacts of Climate Change, Fine Particulate Matter Formation, Water Consumption and Land Use. *Int. J. Life Cycle Assess.* **2018**, *23*, 2189−2207.
(10) Myhre, G.; Shindell, D.; Bréon, F.-M.; Collins, W.; Fuglestvedt, J.; Huang, J.; Koch, D.; Lamarque, J.-F.; Lee, D.; Mendoza, B.; Nakajima, T.; Robock, A.; Stephens, G.; Takemura, T.; Zhang, H. Anthropogenic and Natural Radiative Forcing. In *Climate Change 2013: The Physical Science Basis. Contribution of Working Group I to the Fifth Assessment Report of the Intergovernmental Panel on Climate Change*. Cambridge University Press; Stocker, T. F., Qin, D., Plattner, G.-K., Tignor, M., Allen, S. K., Boschung, J., Nauels, A., Xia, Y., Bex, V., Midgley, P. M., Eds.; Cambridge University Press: Cambridge, 2013.
(11) Bjørn, A.; Hauschild, M. Z. Introducing Carrying Capacity-Based Normalisation in LCA: Framework and Development of References at Midpoint Level. *Int. J. Life Cycle Assess.* **2015**, *20* (7), 1005−1018.
(12) Levasseur, A.; Cavalett, O.; Fuglestvedt, J. S.; Gasser, T.; Johansson, D. J. A.; Jørgensen, S. V.; Raugei, M.; Reisinger, A.; Schivley, G.; Strømman, A.; Tanaka, K.; Cherubini, F. Enhancing Life Cycle Impact Assessment from Climate Science: Review of Recent Findings and Recommendations for Application to LCA. *Ecol. Indic.* **2016**, *71*, 163−174.
(13) Jørgensen, S. V.; Hauschild, M. Z.; Nielsen, P. H. Assessment of Urgent Impacts of Greenhouse Gas Emissions - The Climate Tipping Potential (CTP). *Int. J. Life Cycle Assess.* **2014**, *19* (4), 919−930.
(14) Lenton, T. M.; Ciscar, J.-C. Integrating Tipping Points into Climate Impact Assessments. *Clim. Change* **2013**, *117* (3), 585−597.
(15) Drijfhout, S.; Bathiany, S.; Beaulieu, C.; Brovkin, V.; Claussen, M.; Huntingford, C.; Scheffer, M.; Sgubin, G.; Swingedouw, D. Catalogue of Abrupt Shifts in Intergovernmental Panel on Climate Change Climate Models. *Proc. Natl. Acad. Sci. U. S. A.* **2015**, *112* (43), E5777−E5786.
(16) de Haes, H. A. U.; Jolliet, O.; Finnveden, G.; Hauschild, M.; Krewitt, W.; Muller-Wenk, R. Best Available Practice Regarding Impact Categories and Category Indicators in Life Cycle Impact Assessment. *Int. J. Life Cycle Assess.* **1999**, *4* (2), 66−74.
(17) Heijungs, R. Is Mainstream LCA Linear? *Int. J. Life Cycle Assess.* **2020**, *25* (10), 1872−1882.
(18) Boulay, A.-M.; Benini, L.; Sala, S. Marginal and Non-Marginal Approaches in Characterization: How Context and Scale Affect the Selection of an Adequate Characterization Factor. The AWARE Model Example. *Int. J. Life Cycle Assess.* **2020**, *25*, 2380−2392.
(19) Huijbregts, M. A. J.; Hellweg, S.; Hertwich, E. Do We Need a Paradigm Shift in Life Cycle Impact Assessment? *Environ. Sci. Technol.* **2011**, *45* (9), 3833−3834.
(20) Heijungs, R. The Average versus Marginal Debate in LCIA: Paradigm Regained *Int. J. Life Cycle Assess.* **2020**. DOI: 10.1007/s11367-020-01835−4.
(21) Bjørn, A.; Diamond, M.; Owsianiak, M.; Verzat, B.; Hauschild, M. Z. Strengthening the Link between Life Cycle Assessment and Indicators for Absolute Sustainability to Support Development within Planetary Boundaries. *Environ. Sci. Technol.* **2015**, *49* (11), 6370−6371.
(22) Bjørn, A.; Chandrakumar, C.; Boulay, A. M.; Doka, G.; Fang, K.; Gondran, N.; Hauschild, M. Z.; Kerkhof, A.; King, H.; Margni, M.; McLaren, S.; Mueller, C.; Owsianiak, M.; Peters, G.; Roos, S.; Sala, S.; Sandin, G.; Sim, S.; Vargas-Gonzalez, M.; Ryberg, M. Review of Life-Cycle Based Methods for Absolute Environmental Sustainability Assessment and Their Applications *Environ. Res. Lett.* **2020**, *15* (8). 083001.
(23) Bjørn, A. (DTU). Better, but Good Enough? Indicators for Absolute Environmental Sustainability in a Life Cycle Perspective. Technical University of Denmark, DTU Management Engineering. PhD Thesis, No. 8.2015, 2015.
(24) van Vuuren, D. P.; Edmonds, J.; Kainuma, M.; Riahi, K.; Thomson, A.; Hibbard, K.; Hurtt, G. C.; Kram, T.; Krey, V.; Lamarque, J.-F.; Masui, T.; Meinshausen, M.; Nakicenovic, N.; Smith, S. J.; Rose, S. K. The Representative Concentration Pathways: An Overview. *Clim. Change* **2011**, *109* (1−2), 5−31.
(25) Meinshausen, M.; Smith, S. J.; Calvin, K.; Daniel, J. S.; Kainuma, M. L. T.; Lamarque, J.; Matsumoto, K.; Montzka, S. A.; Raper, S. C. B.; Riahi, K.; Thomson, A.; Velders, G. J. M.; van Vuuren, D. P. P. The RCP Greenhouse Gas Concentrations and Their Extensions from 1765 to 2300. *Clim. Change* **2011**, *109* (1), 213−241.
(26) Sanford, T.; Frumhoff, P. C.; Luers, A.; Gulledge, J. The Climate Policy Narrative for a Dangerously Warming World. *Nat. Clim. Change* **2014**, *4* (3), 164−166.
(27) van Vliet, J.; den Elzen, M. G.J.; van Vuuren, D. P. Meeting Radiative Forcing Targets under Delayed Participation. *Energy Econ.* **2009**, *31*, S152−S162.
(28) Meinshausen, M.; Wigley, T. M. L.; Raper, S. C. B. Emulating Atmosphere-Ocean and Carbon Cycle Models with a Simpler Model, MAGICC6 − Part 2: Applications. *Atmos. Chem. Phys.* **2011**, *11*, 1457−1471.
(29) Levasseur, A.; Lesage, P.; Margni, M.; Deschĕnes, L.; Samson, R. Considering Time in LCA: Dynamic LCA and Its Application to Global Warming Impact Assessments. *Environ. Sci. Technol.* **2010**, *44* (8), 3169−3174.
(30) Tansel, B. Persistence Times of Refractory Materials in Landfills: A Review of Rate Limiting Conditions by Mass Transfer and Reaction Kinetics. *J. Environ. Manage.* **2019**, *247*, 88−103.
(31) Ishigaki, T.; Sugano, W.; Nakanishi, A.; Tateda, M.; Ike, M.; Fujita, M. The Degradability of Biodegradable Plastics in Aerobic and Anaerobic Waste Landfill Model Reactors. *Chemosphere* **2004**, *54*, 225−233.
(32) Cho, H. S.; Moon, H. S.; Kim, M.; Nam, K.; Kim, J. Y. Biodegradability and Biodegradation Rate of Poly (Caprolactone) -Starch Blend and Poly (Butylene Succinate) Biodegradable Polymer under Aerobic and Anaerobic Environment. *Waste Manage.* **2011**, *31* (3), 475−480.
(33) Rossi, V.; Cleeve-Edwards, N.; Lundquist, L.; Schenker, U.; Dubois, C.; Humbert, S.; Jolliet, O. Life Cycle Assessment of End-of-Life Options for Two Biodegradable Packaging Materials: Sound Application of the European Waste Hierarchy. *J. Cleaner Prod.* **2015**, *86*, 132−145.
(34) JRC. *International Reference Life Cycle Data System (ILCD) Handbook − General Guide for Life Cycle Assessment − Detailed Guidance*. Publications Office of the European Union; Ispra. Luxembourg, 2010.
(35) Levasseur, A.; Lesage, P.; Margni, M.; Samson, R. Biogenic Carbon and Temporary Storage Addressed with Dynamic Life Cycle Assessment. *J. Ind. Ecol.* **2013**, *17* (1), 117−128.
(36) Hansen, J.; Sato, M.; Kharecha, P.; Von Schuckmann, K. Earth's Energy Imbalance and Implications. *Atmos. Chem. Phys.* **2011**, *11* (24), 13421−13449.
(37) Kriegler, E.; Hall, J. W.; Held, H.; Dawson, R.; Schellnhuber, H. J. Imprecise Probability Assessment of Tipping Points in the Climate System. *Proc. Natl. Acad. Sci. U. S. A.* **2009**, *106* (13), 5041−5046.
(38) Rocha, J. C.; Peterson, G.; Bodin, Ö.; Levin, S. Cascading Regime Shifts within and across Scales. *Science (Washington, DC, U. S.)* **2018**, *362*, 1379−1383.
(39) Owsianiak, M.; Brooks, J.; Renz, M.; Laurent, A. Evaluating Climate Change Mitigation Potential of Hydrochars: Compounding Insights from Three Different Indicators. *GCB Bioenergy* **2018**, *10* (4), 230−245.

https://dx.doi.org/10.1021/acs.est.0c02928
Environ. Sci. Technol. 2021, 55, 2800−2810

Science of the Total Environment 788 (2021) 147544

Contents lists available at ScienceDirect

Science of the Total Environment

journal homepage: www.elsevier.com/locate/scitotenv

Inclusion of multiple climate tipping as a new impact category in life cycle assessment of polyhydroxyalkanoate (PHA)-based plastics

Eldbjørg Blikra Vea [a,*], Serena Fabbri [a], Sebastian Spierling [b], Mikołaj Owsianiak [a]

[a] Division for Sustainability, Department of Technology, Management and Economics, Technical University of Denmark, Produktionstorvet, Building 424, DK-2800 Kongens Lyngby, Denmark
[b] Institute of Plastics and Circular Economy, Leibniz Universität Hannover, An der Universität 2, 30823 Garbsen, Germany

HIGHLIGHTS

- LCA applied to PHA with improved barrier properties.
- Inclusion of new impact category, the multiple climate tipping.
- PHA films with high biodegradability perform best.
- Multiple climate tipping is a relevant impact category for LCA of PHA.

GRAPHICAL ABSTRACT

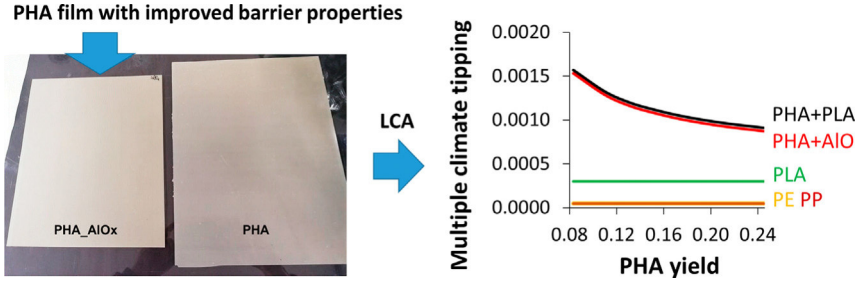

ARTICLE INFO

Article history:
Received 1 March 2021
Received in revised form 13 April 2021
Accepted 30 April 2021
Available online 11 May 2021

Editor: Deyi Hou

Keywords:
Bioplastic
Circular economy
Climate tipping points
Sustainability
Waste management

ABSTRACT

The merits of temporary carbon storage are often debated for bio-based and biodegradable plastics. We employed life cycle assessment (LCA) to assess environmental performance of polyhydroxyalkanoate (PHA)-based plastics, considering multiple climate tipping as a new life cycle impact category. It accounts for the contribution of GHG emissions to trigger climate tipping points in the Earth system, considering in total 13 tipping elements that could pass a tipping point with increasing warming. The PHA was either laminated with poly(lactic acid), or metallized with aluminum or aluminum oxides to lower permeability of the resulting plastics toward oxygen, water vapor and aromas. The assessments were made accounting for potential differences in kinetics of evolution of greenhouse gases (CO_2, CH_4) from bioplastic degradation in the end-of-life. Results show that: (1) PHA films with high biodegradability perform best in relation to the climate tipping, but are not necessarily the best in relation to radiative forcing increase or global temperature change; (2) sugar beet molasses used as feedstock is an environmental hot spot, contributing significantly to a wide range of environmental problems; (3) increasing PHA production scale from pilot to full commercial scale increases environmental impacts, mainly due to decreasing PHA yield; and (4) further process optimization is necessary for the PHA-based plastics to become attractive alternatives to fossil-based plastics. Our study suggests that multiple climate tipping is a relevant impact category for LCA of biodegradable bioplastics.

1. Introduction

Bioplastics are a diverse group of materials which have been in the focus of research as alternative to conventional plastics (Spierling et al., 2018; García et al., 2019; Kookos et al., 2019; Pavan et al., 2019; Rameshkumar et al., 2020). Bioplastics consist of three sub-categories and can either be (1) "fossil-based and biodegradable", (2) "bio-based

* Corresponding author.
E-mail addresses: ebve@dtu.dk (E.B. Vea), serf@dtu.dk (S. Fabbri), spierling@ikk.uni-hannover.de (S. Spierling), miow@dtu.dk (M. Owsianiak).

https://doi.org/10.1016/j.scitotenv.2021.147544

and biodegradable" or (3) "bio-based and non-biodegradable". The last two categories can also be combined with the term bio-based plastics (Endres and Siebert-Raths, 2011). The market share of bioplastics is predicted to continue to grow within the next years to 2.8 Mio. tonnes in 2025, an increase of 35% compared to the production capacities in 2020 (European Bioplastics, 2020b).

This study focuses on production of polyhydroxyalkanoate (PHA) from sugar beet molasses. PHA is a bio-based and biodegradable polyester which can be produced by bacterial fermentation (Chen et al., 2020; Moretto et al., 2020). The PHAs are produced as intracellular high-molecular inclusion bodies, which have a role as carbon- and energy storage compounds within the bacteria. The selection of different microbial production strains as well as adaptions of the bioprocess allows the composition of different PHA types (homo-, co-, ter-, and quad-polyesters), resulting in up to 150 different PHA structures which have been identified so far. Based on their carbon atoms used for the monomeric unit PHAs can be differentiated in two main groups: (1) short-chain-length PHAs with 3–5 carbon atoms and (2) medium-chain-length PHAs with 6–14 carbon atoms. The most well-known and common PHA type is poly-β-hydroxybutyrate (PHB) (Koller, 2017; Kourmentza et al., 2017; Troschl et al., 2018). Additionally, for the production of PHA, a wide range of feedstocks can be utilized. E.g. renewable materials like sugar, industrial waste and by-product streams, as well as CO_2, which can be utilized by cyanobacteria types (Koller, 2017; Kookos et al., 2019; Moretto et al., 2020; Wongsirichot et al., 2020). This makes PHA a versatile plastic type within the bioplastics and bio-based plastics.

A number of international patents about plastic materials based on PHA have been obtained (Elvers et al., 2016 and references therein). Yet, global production of PHA is relatively low (25,320 tons in year 2019), accounting for only 1.2% of the bioplastics market (Rameshkumar et al., 2020). The reason for the low market share of PHAs is mainly due to high production costs (García et al., 2019; Kookos et al., 2019; Pavan et al., 2019), that are estimated to be 5–10 times higher than the cost of traditional polymers (Kookos et al., 2019). The latest market data for PHA predicts an increase to 11.5% of the bioplastics market till 2025 (European Bioplastics, 2020a). Currently PHA is manufactured worldwide at both pilot and industrial scale. Manufacturers are based in Canada, Germany, Italy, China, USA, Japan as well as Malaysia. On these scales mainly first-generation feedstock like sugar (e.g. from sugar beet) as well as vegetable oil (e.g. canola oil or palm oil) is dominant (Kourmentza et al., 2017). Molasses, a co-product of sugar beet, is often considered as feedstock for PHA production (Baei et al., 2009; Keunun et al., 2018; Kiran Purama et al., 2018; Remor Dalsasso et al., 2019). Molasses contains about 50% of the disaccharide sucrose and is commonly used as an energy supplement to livestock feed. PHA exhibits physical and mechanical properties similar to those of conventional plastics, such as polyethylene (PE) and polypropylene (PP) (Kookos et al., 2019).

One potential application of PHA is as food packaging material (Khosravi-Darani and Bucci, 2015). For example, bioplastic is considered for packaging of high quality bakery products, replacing fossil based polypropylene. Yet, high permeability toward water, oxygen and aromas makes PHA a rather poor packaging material (Kassavetis et al., 2012). It is thus necessary to improve the barrier properties to lower permeability if PHA is to be used in contact with food (Struller et al., 2014). This can be done by lamination with (poly)lactic acid (PLA) or metallization with aluminum (Al) or aluminum oxides (AlOx) (Kassavetis et al., 2012). Until now, nothing was known about sustainability implications of lamination or metallization of PHA, which improve barrier properties but may impair biodegradability in their end-of-life. Environmental assessments of PHA production from molasses generally focused on the fermentation and PHA recovery steps, without considering other important process in the PHA-based plastic film life cycle like post-treatment and end-of-life (Leong et al., 2017; Kookos et al., 2019).

The purpose of this paper was to assess the environmental performance of the whole value chain of PHA-based plastics with improved barrier properties. We considered lamination using PLA or metallization using Al or AlOx as two viable surface treatment options. The environmental performance was assessed using life cycle assessment (LCA). To provide additional insights to the metrics of climate change recommended in the EU Commission's ILCD Handbook (ISO, 2006; EC-JRC, 2010) (the global warming potential, GWP_{100}, and the global temperature change potential, GTP_{100}), we present the inclusion of a new life cycle impact category, the multiple climate tipping (Fabbri et al., 2021). It accounts for the contribution of GHG emissions to trigger multiple climate tipping points in the earth system (up to 13 tipping points).

2. Methods

2.1. Scenarios

Molasses, a by-product from sugar beet refinery rich in the carbohydrate sucrose, was chosen as a feedstock and the Gram-negative bacterium *Ralstonia eutropha* as fermenting microbe because they were found promising for full scale applications (Baei et al., 2009; BioBarr, 2019; Remor Dalsasso et al., 2019). Both pilot and large scale were modelled and compared. They differ in capacity (about 100 and 9000 tones PHA recovered per year in the pilot and large scale plants, respectively), and in means of how feedstock is collected, pre-treated, fermented, recovered and purified. In addition to testing the influence of plant scale, we considered differences in (i) geographic location of the PHA plant, (ii) conventional use of molasses, (iii) composition of PHA-based films and other packaging materials, (iv) yield of PHA in the fermentation process, (v) thickness of the PHA layer, and (vi) fate of the improved bioplastic in its end-of-life. Production of poly-β-hydroxybutyrate (PHB) was modelled.

Italy and Germany were chosen as two representatives of countries where production of PHA is currently conducted. Differences in electricity grid mixes and waste management systems between the countries were considered. The waste management systems were modelled according to country-specific rates for recycling, incineration and landfilling of plastic packaging (Eurostat, 2017). Bioplastic packaging is currently not recyclable. Thus, it was assumed that the remaining fraction was treated proportionally to the treatment of non-recovered plastic waste (that is, 50% landfilled and 50% incinerated in Italy and 100% incinerated in Germany). The conventional use of molasses is as animal feed, however, it can be also used for ethanol production (Takriti et al., 2017) and these two scenarios were also explored. We investigated optimization potentials for PHA-based plastics made from molasses, which lie in selection of the material for lowering permeability of the PHA (either PLA or Al or AlOx), optimizing PHA production yield and reducing thickness of the plastic layers. The PHA-based plastics were compared with fossil-based alternatives, namely PP and PE. Comparisons were also made with PLA. Merits of temporary carbon storage are often debated for bioplastics, and the end-of-life stage of the plastics life cycle is the only stage where temporal carbon storage can occur. PHA is generally considered as readily biodegradable (the actual duration of degradation depends on product dimensions as well as environmental parameters like temperature), but it is currently unknown how improving barrier properties influences biodegradability during landfilling (Emadian et al., 2017; Meereboer et al., 2020). Thus, fast degradation was assumed in the baseline scenario. Delayed biodegradation may be caused by differences in availability of water and oxygen during landfilling (Meereboer et al., 2020). Moreover, combining PHA with PLA has shown to reduce biodegradability of PHA (Meereboer et al., 2020). To explore sensitivities toward mineralization rates, different biodegradation rates and extents of lag phases were explored for the landfilling scenarios. We conservatively assumed that no PHA plastic is lost to the environment owing to generally sound

management of plastic waste in Europe (Ryberg et al., 2019). In total, 53 scenarios were considered (refer to Table S3S3, Section S2 of SI for an overview of all scenarios).

2.2. Literature review

Parameters and installations for fermentation, recovery and purification of PHA at pilot and large scales were modelled based on parameters retrieved from scientific literature, identified through a systematic literature review (see Section S1 of the SI for further details). The review encompassed studies focusing on both technical and environmental aspects of PHA production. It was carried out using Scopus in March 2020, applying a set of keyword strings. We retrieved those studies, which: (i) report parameters relevant for the PHA production (feedstock type and its water content, producing microorganism, plant scale and capacity), (ii) are either at pilot (as defined by the study itself or between 10 and 1000 L fermenter volume) or large (above 1000 L) scales, and (iii) either report PHA yield ($kg_{PHA}/kg_{feedstock}$), or sufficient data to estimate the yield. In total, 25 studies were retrieved. We found four studies which use disaccharides, and report data on resource consumptions (e.g. electricity, water and chemicals) (see Table S2 in Section S1). These four studies were used for extraction of parameters and bills of materials needed to model PHA production installations in our LCA.

2.3. Overview of PHA installations

The pilot and large scale systems differ in how feedstock collection, pre-treatment and fermentation, recovery and purification are carried out (see Section S2 of the SI, Fig. S1 for an overview of their installations). The remaining steps are the same and represent large-scale systems. The feedstock is transported by truck at pilot scale, whereas at large scale the feedstock is transported using pipes. At both scales, the feedstock is sterilized by steam and the sterilized feedstock is cooled down using a heat exchanger. At pilot scale, the sterilized feedstock is fermented in one 10-m^3 reactor for 80 h. At large scale, three 102-m^3 reactors for 54 h are used. Electricity input for aeration and agitation are different for the two scales. Fermentation yield is higher at pilot than at large scale (0.360 and 0.268 $kg_{PHA}/kg_{substrate}$, respectively). At both scales, PHA is extracted from fermenting cells and purified in a sequence of steps, involving centrifugation and spray drying, but electricity inputs are higher and consumption of materials generally lower at the pilot scale. Hydrochloride is used for extraction at pilot scale, while hydrogen peroxide and enzymes are used at large scale. The obtained PHA powder is compounded and blended with additives (plasticize, nucleating agent, stabilizer and reinforcing filler) before extruding it into PHA pellets. These pellets are subsequently extruded into a PHA film. This film is either laminated with a layer of PLA, or metallized using aluminum. The aluminum layer can be optionally oxidized to aluminum oxide (AlOx) to make the resulting film transparent. Details of the parameters underlying LCA model are presented in the SI, Section S2.

2.4. Life cycle assessment

The environmental performance was assessed using life cycle assessment (LCA) conducted in accordance with the requirements of the ISO 14044 standard and the guidelines of the EU Commission's ILCD Handbook (ISO, 2006; EC-JRC, 2010).

2.4.1. Functional unit and reference flow

The primary function of the PHA-based bioplastic in the context of this study is to protect dry food against environment during transport and storage. We choose a croissant as an exemplar of dry food product. The functional unit was therefore defined as "Protection of one average croissant (ca. 40 g) against migration of oxygen, water and aromas (according to global and specific migration standards BS EN 1186 and UNE-EN 13130 for migration of aromatic primary amines, pthalic acid, crotonic acid, acrylic acid and the elements Al, B, Ba, Cu, Co, Fe, Li, Mn, Ni and Zn) during transport and storage for 30 days". This functional unit was chosen as it allows a consistent comparison with alternative plastics used as packaging materials. The reference flow is equal to 0.06384 m^2 of PHA-based plastic film with improved barrier properties, and the same reference flows apply to other plastics fulfilling this functional unit. Yet, differences in thicknesses of the PHA based plastic films and other plastics result in different reference flows when expressed on a mass basis.

2.4.2. Modelling framework and system boundaries

Production of PHA-based bioplastic with improved barrier properties and its use in food supply is a relatively new technology and its implementation is not expected to cause large scale market consequences (for example the need to install new power plants). Therefore, consistent with ILCD's recommendations, the current LCA is considered a microlevel decision support situation (type A) (EC-JRC, 2010). This implies that: (i) system expansion is the preferred way to solve multifunctionality, and (ii) average processes are to be used to model the background system of the study. The consequential version of the ecoinvent v3.5 database was employed to model the background system because it prioritizes system expansion rather than allocation (Bjørn et al., 2017). However, this consequential database systematically uses marginal processes rather than average ones. Therefore, to make the database more consistent with the attributional approach, some processes were adapted to be based on average rather than marginal mixes. Details on these adaptations are presented in SI, Section S2 (Table S9). For example, as in (Bohnes, 2020), the marginal electricity grid mix originally included in the consequential database was adapted to represent the average mix of 2018. The use of marginal data was considered negligible for other processes in the bioplastic life cycle and their adaptation was not deemed necessary. The product systems were modelled in SimaPro, version 8.3.0.0 (PRé Consultants B.V., the Netherlands).

An overview of system boundaries, specifying processes included in the LCA, is presented in Fig. 1. Background processes include (avoided) conventional use of the feedstock, production of energy and chemicals, construction and disposal of equipment, and treatment of biological waste. The use stage includes transport from production site to the customer. The end-of-life stage comprises waste management processes according to the waste management of system in the country of interest. The foreground system comprises all processes, as presented in Fig. 1. Molasses is a residual product from production of sugar and therefore no burdens are attributed to its production. However, environmental burdens occur when the molasses waste stream is diverted for production of PHA, rather than its conventional use as animal feed. Consistently with system expansion being prioritized over allocation when handling multifunctional processes, this animal feed has to be produced from other sources, like barley grains.

2.4.3. Life cycle impact assessment

Environmental impact scores were mainly calculated using ReCiPe 2016 as LCIA methodology, applying midpoint indicators and hierarchist perspective. Impact scores were calculated for all ReCiPe impact categories, except climate change which was replaced by the approach of ILCD (2011) combined with updated GWP100 values from IPCC AR5 (IPCC, 2014). The ILCD (2011) approach was preferred as it gives credits to delayed emissions of greenhouse gases (GHGs), which are particularly relevant for the end-of-life stage of the PHA-based plastics. In addition to the GWP100, which is the default metric in LCA and addresses short/medium term climate impacts, we employed the global temperature change potential (GTP100) and the multiple climate tipping points potentials (MCTPs) as characterization factors (CFs). The GTP100 is recommended for use in LCA, next to the GWP100, as it focuses on long-term impacts, representing global average temperature increase of the atmosphere at 100 years that results from the emission

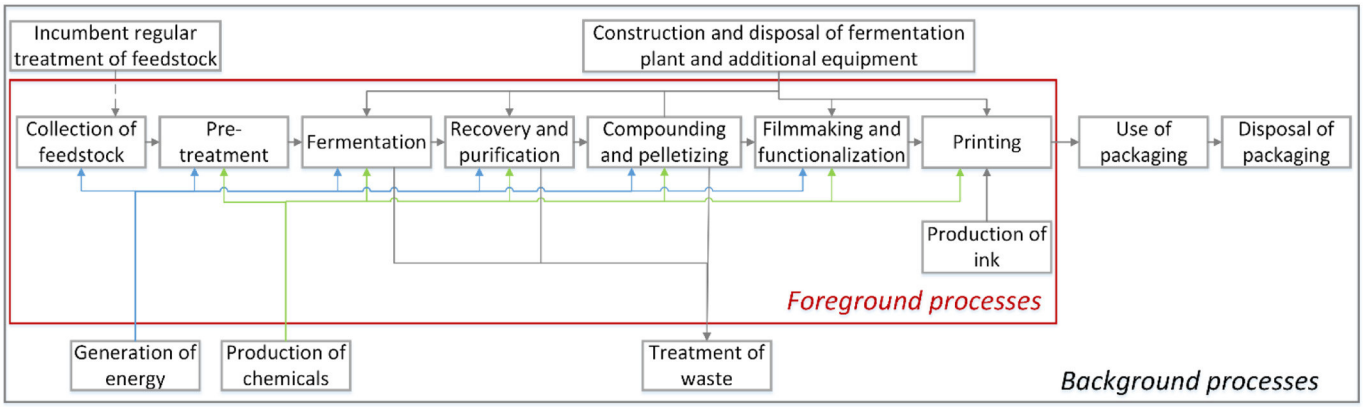

Fig. 1. System boundaries of the PHA-based plastics with improved barrier properties.

(Shine et al., 2005; Levasseur et al., 2016). The MCTP is a recently developed metric for climate tipping impacts (Fabbri et al., 2021), building on earlier work of Jørgensen et al. (2013). It specifically addresses the potential contribution of GHG emissions to trigger multiple climate tipping points in the earth system (like loss of Arctic summer sea ice or the El Niño-southern oscillation intensification), considering in total 13 tipping elements that could pass a tipping point with increasing warming. The contribution to tipping is measured as the share of remaining carrying capacity up to each tipping point that is consumed by the emissions, using Eq. (1) (Fabbri et al., 2021), and is expressed as fraction of depleted remaining capacity in parts per trillion, ppt_{rc}, per kg GHG emission:

$$MCTP_i(T_{\text{emission}}) = \sum_{j=1}^{m} \frac{I_{\text{emission},i,j}\,(T_{\text{emission}})}{CAP_j\,(T_{\text{emission}})} \quad (1)$$

where $MCTP_i(T_{\text{emission}})$ is the characterization factor for GHG i emitted at time T_{emission}, j is the jth out of m potentially exceeded tipping points, $I_{\text{emission},\,i,\,j}$ is the increase in CO_2-equivalent concentration caused by the emission with respect to tipping point j, and CAP_j is the remaining capacity of the atmosphere to absorb this concentration increase without triggering tipping point j (Fabbri et al., 2021). Given that the MCTP is sensitive to the timing of emissions, the metric is particularly relevant for the end-of-life of PHA-based plastics, as emissions are distributed over time and could contribute to crossing tipping points (Fabbri et al., 2021). The three climate-related sets of indicators are complementary to each other and represent three different impact categories. Details of calculation of impact scores using these three approaches are presented in Section S3 of the SI.

2.5. Sensitivity and uncertainty analyses

Sensitivities of the LCA results to discrete parameters were evaluated in a scenario analysis (see Section 2.1). Sensitivities to PHA yield, which is a continuous parameter, was also considered for selected scenarios from Table S3S3, Section S2 of SI. Quantification of inventory uncertainties is currently not possible to carry out with the consequential version of the ecoinvent database as attached to SimaPro. To compensate for this limitation, we conducted a qualitative uncertainty analysis discussing limitations of the study considering the specificity of the inventory data.

3. Results and discussion

In the following sections, we present an overview of life cycle impact assessment results for selected scenarios, identify factors which determine overall environmental performance of the PHA plastics, and identify optimization potentials.

3.1. Environmental hot-spots in the PHA value chain

To identify processes with the largest contribution to this burden, process contribution analysis was carried out on PHA laminated with PLA at pilot and large scale systems in Italy (Fig. 2). Refer to Table S13, Section S4 of the SI for tabulated impact scores for the two scenarios. Irrespective of the plant scale, incumbent management of feedstock had the highest contribution to environmental burden for most, but not all, impact categories (up to 94% of total impact, depending on the impact category). As explained in Section 2.4.2, we consider that when molasses is used for PHA production rather than its incumbent use as animal feed, this animal feed has to be produced from other sources, like barley grains. Thus, relatively high contribution of incumbent management of feedstock is explained by burdens associated with production of animal feed from barley grains. Negative impact scores (indicating environmental benefits) are observed for the climate change impact category. They are a result of fixation of CO_2 during cultivation of barley grains. These environmental benefits are, however, outweighed by the burden stemming from the fermentation itself which uses energy and emits CO_2, treatment of wastewater, and incineration of plastic waste in the end-of-life treatment.

The fermentation had relatively small contribution (up to 8% of total impact), except the three climate-related impact categories where its contribution ranged from 21 to 64% of the total impact. The post-treatment processes (recovery, purification, compounding and pelletizing), however, altogether contributed up to 60% of the total impact, depending on the impact category. Previous studies on PHA production from sucrose (including collection, pre-treatment, fermentation and PHA recovery), reported global warming impacts which were higher (1.96 kg CO_2 eq/kg $PHA_{recovered}$ in Harding et al. (2007)) and lower (−2.58 kg CO_2 eq/kg $PHA_{recovered}$ in Kookos et al. (2019) owing to energy recovery from bagasse), compared to 0.76 CO_2 eq/kg $PHA_{recovered}$ in the large scale system of this study. As in Kookos et al. (2019), direct emissions of CO_2 during fermentation were important contribution to climate change burdens in our study. Harding et al. (2007), on the other hand highlighted steam and electricity use as the most contributing process. Further, while our study showed that surfactant had a high contribution to global warming impacts (in our LCA modelled as non-ionic surfactant), neither Harding et al. (2007) nor Kookos et al. (2019) found that the surfactant was the hot spot. Compared to the former study, the consumption of surfactant in our study was 16 times higher, while Kookos et al. (2019) applied a negative GHG emission factor for surfactant based on data from Akiyama et al. (2003).

Relatively high contribution of recovery and purification was mainly caused by the use of steam for spray drying in the pilot system and

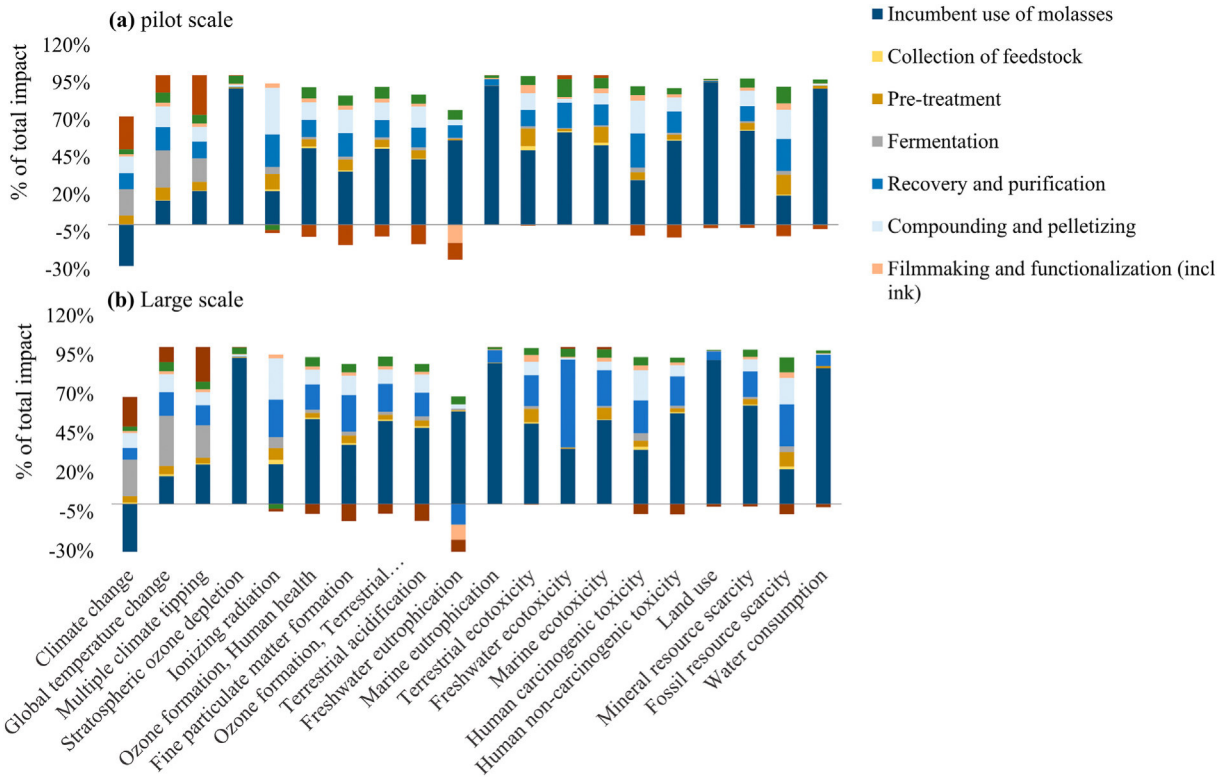

Fig. 2. Contribution of life cycle processes to total impacts from PHA-based packaging at pilot and large scale. The scores for each impact category are scaled to 100%.

surfactant in the large scale system. Surfactant contributed to 55, 24 and 15% of total freshwater ecotoxicity, fossil resource scarcity and climate change impacts. Negative contributions to total impact scores on freshwater eutrophication observed in our study for recovery and purification and filmmaking and functionalization are unexpected, but can be explained by system expansion mechanisms occurring in non-ionic surfactant applied during recovery and purification and ink applied in filmmaking and functionalization processes.

Electricity consumption for processing of the recovered PHA into PHA pellets explains 23 and 19% of total impact for climate change and human carcinogenic toxicity. Negative impact scores for waste management systems for several other impact categories, indicating environmental benefits, were due to incineration with energy recovery (61% of the packaging is incinerated in Italy), substituting production of energy (in this case, electricity and heat for reuse in municipal waste incineration).

3.2. Effects of upscaling

The large scale system has slightly higher impact scores than the pilot scale one consistently for all impact categories, except climate change and freshwater eutrophication (Table S13, Section S4). The largest differences were observed for freshwater ecotoxicity followed by, water consumption, land use and marine eutrophication, where large scale production shows impacts from ~1.5 to ~2.5 times higher than at pilot scale, respectively. This finding was unexpected, because upscaling of technologies is often associated with decreasing environmental impacts perf unit of output (although generalization across different technologies cannot be made) (Gavankar et al., 2015; Owsianiak et al., 2016). The different result in our case can be explained by differences in environmental performance of; (i) recovery and purification steps (all impact categories, except climate change and stratospheric ozone depletion), (ii) fermentation (all impact categories), (iii) collection of feedstock fermentation (all impact categories) and (iv) incumbent use of molasses (all impact categories, except climate change). Increased impacts for recovery and purification were due to higher consumption of surfactant in the large scale system, particularly so for freshwater ecotoxicity where the large scale systems shows 7.7 times higher impact. This increase outweighed benefits from a lower electricity and steam consumption in the large scale. Increasing impacts from fermentation were mainly due to a higher electricity consumption for aeration. Furthermore, slightly lower yield in the large scale system resulted in higher consumption and collection of molasses per unit of PHA output, increasing impacts. Similar, the lower yield at large scale increased incumbent use of molasses and impacts for all categories except climate change where increased amount of CO_2 fixated reduced impact scores. By contrast, reduced impacts from pre-treatment were due to lower consumption of steam, but these reductions were generally insufficient make the large-scale system perform better.

3.3. Influence of geographic location and incumbent use of feedstock

Impact scores decreased for 12 out of 20 impact categories when (large-scale) PHA production and functionalization took place in Germany instead of in Italy (see Section S4 of the SI, Fig. S2). The largest differences were for the climate change and multiple climate tipping impact categories (decrease by 32 and 20%, respectively) followed by fine particulate matter formation and terrestrial acidification (decrease by 17 and 16%, respectively). For climate change, the reductions were due differences in waste management systems between the two countries (the majority of plastics is incinerated in Germany, while landfilling is the dominant treatment option in Italy). Incineration is seen beneficial over landfilling because it does not result in emission of potent GHG, methane (71% of carbon is assumed to be released as methane during landfilling (Rossi et al., 2015)). For fine particulate matter and terrestrial acidification, lower impacts in Germany can be explained by a lower portion of oil in the electricity grid mix in Germany (3.7% and 0.9% in Italy and Germany, respectively), which has a high contribution to these impact categories.

Impact scores increased for 13 out of 20 impact categories when molasses was used as feedstock for ethanol production (scenario 5) rather than for animal feed (scenario 2) in Italy. The largest increase was observed for impacts related to mineral resources, human non-carcinogenic toxicity, terrestrial ecotoxicity and global temperature change (increase by 64, 36, 31 and 28%, respectively) (see Section S4 of the SI, Fig. S3). This was due to generally higher environmental impacts from production of ethanol than production of animal feed (per unit of molasses). Substantial reductions in impact scores were seen for freshwater eutrophication, land use and marine eutrophication (decrease by 365, 138 and 94%, respectively), with negative impact scores for the first two categories (-1.6×10^{-5} kg P eq and -4.0×10^{-2} m^2a crop eq, respectively) and low impacts for marine eutrophication (1.1×10–5 kg N eq) in scenario 5. These negative scores were due to handling a waste product from ethanol production from maize by system expansion, replacing soybean meal. Similar observations were made for Germany, where both increases and decreases in impact scores were observed when the incumbent treatment of molasses was as feedstock for ethanol production.

3.4. Influence of PHA stability

Impact scores of the PHA value chain for the three climate-related impact categories are influenced by mineralization kinetics and extent of the mineralization lag phase in landfilling (Table 1). For all three indicators, lowest impact scores were consistently identified for the very slow degradation scenario (scenario 51). This was mainly due to incomplete degradation over 100 year time (GWP and GTP) and over 94 years (MCTP), where only 1% of initial plastic degraded in this scenario, resulting in lower impact scores. Plastics with fast and medium mineralization kinetics generally performed worse according to GWP as credits given for temporary carbon storage are lower compared to more stable plastics. By contrast, climate tipping impact scores increased with decreasing mineralization rates, because the probability that a significant portion of emissions is released in proximity to tipping points, where MCTP values are the largest, was higher for the more stable plastics. This was even more pronounced for cases where a mineralization lag phase of 20 and 40 years was assumed (scenarios 52 and 53 in Table 1). In those cases, a larger share of the emissions was released close to the year 2050, where MCTPs are the highest. Mineralization kinetics was not found to matter for the GTP metric, because this approach disregards any benefits from temporary carbon storage and does not account for when GHG emissions occur in the life cycle.

3.5. Making PHA-based plastics more sustainable

PHA-based plastics can be made more sustainable by optimizing PHA yield, thickness of the PHA layer, and choice of material for ensuring barrier properties. Fig. 3 shows the effects of these parameters on environmental performance for selected impact categories. Comparisons were also made with pure PLA or pure fossil-based PE, and pure fossil-based PP. Increasing PHA yield generally improves environmental performance of the PHA-based packaging. For MCTP, fossil resource scarcity and land use, impacts decreased from 87 to 28% if yield increases from the minimum to the maximum values reported in the literature for PHA made from molasses (i.e. from 0.083 to 0.245 kg $PHA_{raw}/kg_{molasses}$; scenarios 3–18 in Table S3S3, Section S2). However, only a small increase was observed for climate change (by 2%).This relatively small increase was due to the fact that the decreasing fixation of CO_2 (hence increasing impacts with increasing yield), was outweighed by decreased emissions of CO_2 from fermentation and reduced amount of carbon-containing wastewater to be treated (per unit of PHA output).

The results also showed that PHA combined with either Al or AlOx (scenarios 7 and 8) were more sustainable than the PHA combined with PLA (scenario 2). Impact scores were consistently reduced for all impact categories, except for ionizing radiation (Fig. 3 and Table S14 in the SI, Section S4). The reduction was, however, modest (up to 11% for fossil resource scarcity). Despite relatively large differences in environmental impacts per kg of each alternative material (e.g. higher impacts for Al when compared to PLA), significantly less Al or AlOx (10-nm layer) than PLA (20-μm) is needed to fulfill the functional unit, explaining small differences between PLA and Al (or AlOx).

PHA-based plastics can also be made more sustainable if thickness of underlying materials is reduced (while still allowing the packaging to fulfill the function). However, the extent of required improvements is relatively large. For example, thickness of the PHA layer in the PHA/PLA alternative needs to be reduced to ca. 20 μm for this alternative to be able to compete with pure PLA of 91 μm (in terms of climate change and multiple climate tipping). If PHA yield increases, these PHA-based films would be able to compete with PLA of 50 μm thickness (again, assuming that their functional performance parameters are the same). Irrespective of yield and assumed PHA thickness, however, packaging made of PHA generally does not perform as good as PP- and PE- based packaging does (scenarios 11 and 12 in Table S3) (Fig. 3). The differences were by factor of 2 to 5, depending on the impact category, even if high yield and low thickness of PHA were assumed.

4. Limitations and data gaps

This study presents full life cycle inventory and impact assessment results for PHA-based plastics with improved barrier properties. The main limitations of the study relate to: (1) variability and uncertainty in parameters used for modelling life cycle inventories, (2) the choice of LCI database for modelling background system, and (3) deficiencies in impact assessment method.

Table 1
Impact scores per functional unit (f.u.) of the PHA value chain as depending on stability of the PHA plastics in landfilling conditions (mineralization rate constant and extent of mineralization lag phase) and the climate-related impact category. Color shades from green, yellow to red, indicate increasing impact (per impact category). The scenarios tested for stability and degradation are; fast kinetics: 90% degradation in 2 years (100% degraded in 100 years), medium kinetics: 90% degradation in 31 years (99.9% degraded in 100 years), slow kinetics: 90% degradation in 105 years (89% degraded in 100 years), very slow kinetics: 90% degraded in 22,798 years (1% degraded in 100 years), delayed (20): degradation delayed by 20 years, fast kinetics, delayed (40): degradation delayed by 40 years, fast kinetics (see a full overview of scenarios in Table S3, Section S2).

	GWP_{100} (kg CO_2eq/f.u.)	$MCTP_{RCP6}$ (ppt_{re}/f.u.)	GTP_{100} (kg CO_2eq/f.u.)
Fast (scenario 2)	5.25E-02	1.22E-03	1.04E-01
Medium (scenario 49)	4.53E-02	1.40E-03	1.04E-01
Slow (scenario 50)	3.57E-02	1.45E-03	1.03E-01
Very slow (scenario 51)	2.81E-02	9.40E-04	9.31E-02
Fast with 20-yr lag phase (scenario 52)	4.17E-02	4.95E-03	1.04E-01
Fast with 40-yr lag phase (scenario 53)	3.08E-02	4.93E-03	1.04E-01

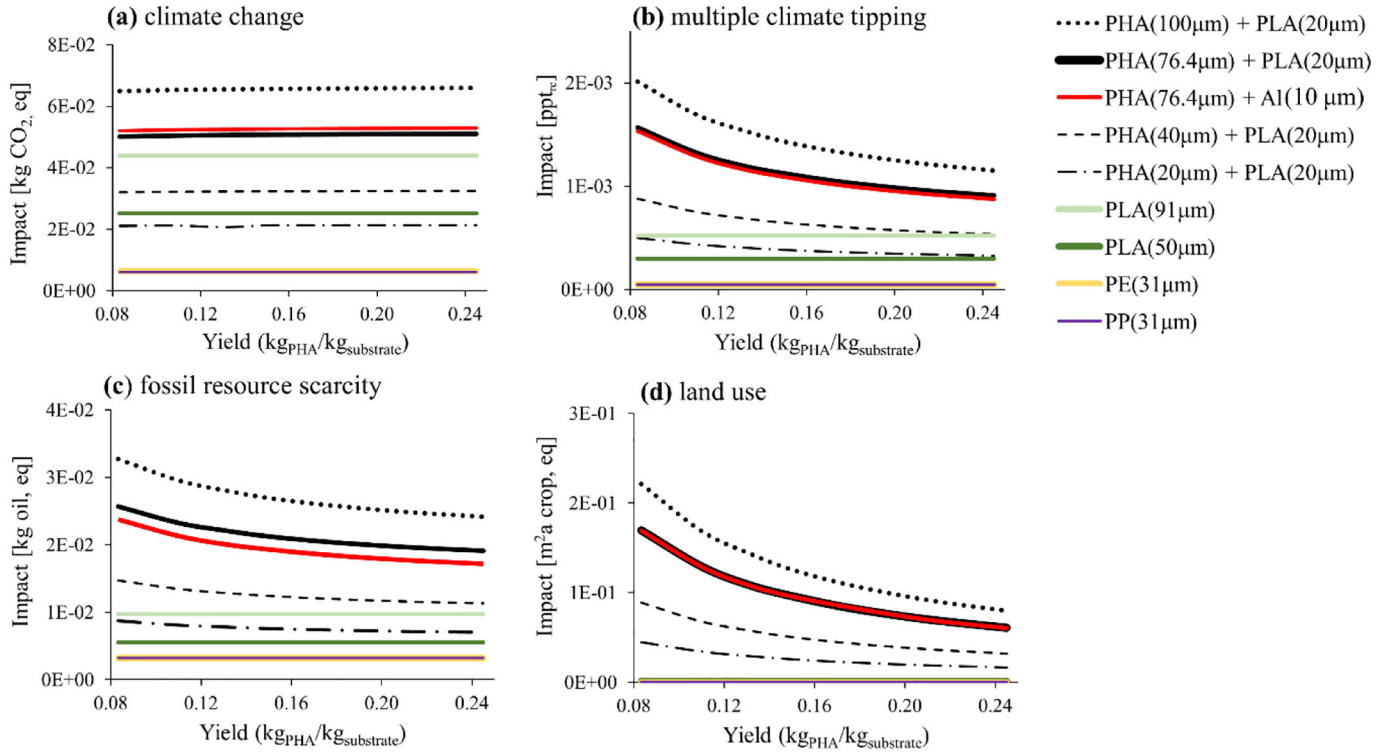

Fig. 3. Impact scores for climate change, multiple climate tipping, fossil resource scarcity and land use as influenced by PHA yield, and type and thickness underlying materials (scenarios 7–48 in Table S3S3, Section S2 of SI). Yields are based on literature data, where the minimum yield is from Kookos et al. (2019) and the maximum yield is estimated from a theoretical yield from Yamane (1993) and assuming that 95% of the accumulated biomass is PHA. The yield in the x-axis refers to PHA-based plastics only. Impacts of PLA, PE and PP are shown in the figure for comparison, but are not influenced by PHA yield.

First, we modelled pilot and large scale PHA production systems basing on data retrieved from the literature, but several parameters are known to be variable or uncertain. This may influence comparisons between scales. For example, PHA yield varies, but is an important parameter which determines performance of the PHA vale chain, and the large scale system would generally perform better than the pilot scale if the PHA yield was in higher range of possible values (0.245 $kgPHA_{raw}/kg_{molasses}$) (data not shown).

Second, biodegradation kinetics of the PHA-based plastics in the environment is highly uncertain (Emadian et al., 2017; Meereboer et al., 2020), and furthermore it is unknown how surface treatment may influence biodegradation kinetics in landfilling conditions. Our sensitivity analyzes show that this parameter is important not only for the end-of-life, but for the performance of the whole PHA value chain (in terms of climate change and multiple climate tipping impacts).

Third, the surfactant in the current study was modelled as a generic non-ionic surfactants, which consists of ethylene oxide (66%) and fatty acid (33%) derivatives. Impacts of surfactants vary considerably (Schowanek et al., 2018). For example, if the fatty acid derivate was used, freshwater eutrophication and ecotoxicity impacts would decrease by 114% and 45%, respectively (data not shown). It is therefore important to address this data gap in future studies on PHA.

Fourth, the consequential background database was consistently applied for background processes, with the exception of electricity processes, which were adapted to average grid mixes rather than marginal mixes. The sensitivity of this was tested for incumbent use of molasses and found to have a high influence on the overall results. Although contribution from other processes of the background system is expected to be smaller when compared to energy and avoided incumbent use of molasses, there is some uncertainty as average mixes (rather than marginal mixes) should ideally be used consistently for all processes in the background system.

Finally, owing to the limitations of the ecoinvent database, indirect land use changes (ILUC) were not considered in the PLA value chain (PLA is made from maize). If they were considered, impacts of those PHA-based plastics which include PLA would increase. According to Ögmundarson et al. (2020), e.g., climate change impact for lactic acid from corn could increase by 14% if ILUC are included. Hence, including ILUC would further favor those alternatives which use either Al or AlOx as barrier materials.

5. Implications for PHA value chain

We showed that PHA-based plastics with improved barrier properties have higher environmental impacts than alternative packaging made from PE, PP and potentially even PLA. These results are not surprising given that PHA production is still relatively immature when compared to the aforementioned alternatives. The largest optimization potentials (which are also challenges to PHA technology developers), are: 1) reduction of PHA thickness while maintaining functional properties of the PHA plastic, 2) increase PHA production yield, 3) increase the energy efficiency during compounding and pelletizing, 4) decrease amount and change type of surfactant used in recovery and purification processes, 5) consider feedstock other than molasses, that do not have a highly beneficial alternative treatment and use. Industrial wastewater could be considered as feedstock, as it avoids incumbent management of the wastewater (Heimersson et al., 2014). Furthermore CO_2 could be a promising alternative feedstock for PHA production (Troschl et al., 2018), but separate LCA would be needed to evaluate performance of PHA made from other feedstock. 6) consider alternative end-of-life options. Although the biodegradability of PHA offers aerobic and anaerobic end-of-life pathways in comparison to conventional plastics, recent research results for PLA show that also recycling (e.g. mechanical recycling) is a potential option which can offer additional benefit from an LCA as well as circular economy perspective (Maga et al., 2019; Spierling et al., 2020). Our study may suggest that that Al (or AlOx) is the preferred material to ensure barrier properties. However, unknown influence of the Al layers on biodegradability of PHA in the environment

warrants further studies. Finally, we stress that we have addressed environmental aspects of sustainability, but economic and socially-oriented analyses are required to make more informed decisions about implementing PHA with improved barrier properties as alternative packaging materials.

CRediT authorship contribution statement

Eldbjørg Blikra Vea: Methodology, Investigation, Data curation, Visualization, Writing – original draft. **Serena Fabbri:** Methodology, Data curation, Writing – review & editing. **Sebastian Spierling:** Writing – review & editing, Validation. **Mikołaj Owsianiak:** Conceptualization, Writing – review & editing, Validation, Supervision.

Declaration of competing interest

The authors declare that they have no known competing financial interests or personal relationships that could have appeared to influence the work reported in this paper.

Acknowledgments

We acknowledge the financial support given by the European Commission under Horizon 2020; H2020-BBI-JTI-2016: BioBarr, grant agreement 745586.

Appendix A. Supplementary data

Details of literature review, data underlying LCA model, details of life cycle impact assessment, additional results (Sections S1–S5), Simpro model processes (Section S6) Supplementary data to this article can be found online at https://doi.org/10.1016/j.scitotenv.2021.147544.

References

Akiyama, M., Tsuge, T., Doi, Y., 2003. Environmental life cycle comparison of polyhydroxyalkanoates produced from renewable carbon resources by bacterial fermentation. Polym. Degrad. Stab. 80 (1), 183–194. https://doi.org/10.1016/S0141-3910(02)00400-7.

Baei, M.S., Najafpour, G.D., Younesi, H., Tabandeh, F., Eisazadeh, H., 2009. Poly(3-hydroxybutyrate) synthesis by cupriavidus necator DSMZ 545 utilizing various carbon sources. World Appl. Sci. J. 7 (2), 157–161.

BioBarr, 2019. D2.4 - Report on the 1st Prototype Film.

Bjørn, A., Owsianiak, M., Laurent, A., Olsen, S.I., Corona, A., Hauschild, M.Z., 2017. Scope definition. Life Cycle Assessment: Theory and Practice. Springer International Publishing, pp. 75–116 https://doi.org/10.1007/978-3-319-56475-3_8.

Bohnes, F., 2020. Prospective assessment of the aquaculture sector - national policies and environmental impacts. Degree under the Joint Doctorate Agreement between the Technical University of Denmark and Nanyang Technological University.

Chen, X., Rodríguez, Y., Lópezlópez, J.C., Muñ Oz, R., Ni, B.-J., Rkan Sin, G., 2020. Modeling of Polyhydroxyalkanoate Synthesis From Biogas by Methylocystis Hirsuta. https://doi.org/10.1021/acssuschemeng.9b07414.

EC-JRC, 2010. International Reference Life Cycle Data System (ILCD) Handbook – General guide for Life Cycle Assessment–Detailed guidance, Constraints. European Commission - Joint Research Centre - Institute for Environment and Sustainability https://doi.org/10.2788/38479.

Elvers, D., Song, C.H., Steinbüchel, A., Leker, J., 2016. Technology trends in biodegradable polymers: evidence from patent analysis. Polym. Rev. 56 (4), 584–606. https://doi.org/10.1080/15583724.2015.1125918 Taylor & Francis.

Emadian, S.M., Onay, T.T., Demirel, B., 2017. Biodegradation of bioplastics in natural environments. Waste Manag. 59, 526–536. https://doi.org/10.1016/j.wasman.2016.10.006 Elsevier Ltd.

Endres, H.J., Siebert-Raths, A., 2011. Engineering biopolymers: markets, manufacturing, properties and applications. Engineering Biopolymers: Markets, Manufacturing, Properties and Applications. Hanser https://doi.org/10.3139/9783446430020.

European Bioplastics, 2020a. Global production capacities 2025 by material type, nova-institute. Available at. https://www.european-bioplastics.org/wp-content/uploads/2020/11/Global_Production_Capacities_2025_by_material_type.jpg. (Accessed 4 February 2021).

European Bioplastics, 2020b. Global production capacities of bioplastics, nova-institute. Available at. https://www.european-bioplastics.org/wp-content/uploads/2020/11/Global_Production_Capacity_Total_2020vs2025.jpg. (Accessed 4 February 2021).

Eurostat, 2017. Management of waste by waste management operations and type of material. Available at. https://appsso.eurostat.ec.europa.eu/nui/show.do?dataset=env_wassd&lang=en. (Accessed 19 October 2020).

Fabbri, S., Hauschild, M., Lenton, T., Owsianiak, M., 2021. Multiple climate tipping points metrics for improved sustainability assessment of products and services. Environ. Sci. Technol. (in press). https://pubs.acs.org/doi/10.1021/acs.est.0c02928.

García, C., Alcaraz, W., Acosta-Cárdenas, A., Ochoa, Silvia, 2019. Application of process system engineering tools to the fed-batch production of poly(3-hydroxybutyrate-co-3-hydroxyvalerate) from a vinasses-molasses mixture. Bioprocess Biosyst. Eng. 42, 1023–1037. https://doi.org/10.1007/s00449-019-02102-z.

Gavankar, S., Suh, S., Keller, A.A., 2015. The role of scale and technology maturity in life cycle assessment of emerging technologies: a case study on carbon nanotubes. J. Ind. Ecol. 19 (1), 51–60. https://doi.org/10.1111/jiec.12175 Blackwell Publishing.

Harding, K.G., Dennis, J.S., Blottnitz, H. Von, Harrison, S.T.L., 2007. Environmental analysis of plastic production processes: comparing petroleum-based polypropylene and polyethylene with biologically-based poly- [illegible] -hydroxybutyric acid using life cycle analysis. 130, 57–66. https://doi.org/10.1016/j.jbiotec.2007.02.012.

Heimersson, S., Morgan-sagastume, F., Peters, G.M., Werker, A., Svanstro, M., 2014. Methodological issues in life cycle assessment of mixed-culture polyhydroxyalkanoate production utilising waste as feedstock. 31 (4). https://doi.org/10.1016/j.nbt.2013.09.003.

ILCD, 2011. Recommendations for Life Cycle Impact Assessment in the European Context. First. ed. Joint Research Centre - Institute for Environment and Sustainability, Luxembourg.

IPCC, 2014. In: Core Writing Team, Pachauri, R.K., Meyer, L.A. (Eds.), Climate change 2014: Synthesis report. Contribution of working groups I, II and III to the fifth assessment report of the intergovernmental panel on climate change Geneva, Switzerland. Available at. https://www.ipcc.ch/site/assets/uploads/2018/05/SYR_AR5_FINAL_full_wcover.pdf. (Accessed 30 January 2020).

ISO, 2006. ISO 14044: Environmental Management—Life Cycle Assessment—Requirements and Guidelines. International Organization for Standardization.

Jørgensen, S.V., Hauschild, M.Z., Nielsen, P.H., 2013. Assessment of Urgent Impacts of Greenhouse Gas Emissions-The Climate Tipping Potential (CTP). https://doi.org/10.1007/s11367-013-0693-y.

Kassavetis, S., Logothetidis, S., Zyganitidis, I., 2012. Nanomechanical testing of the barrier thin film adhesion to a flexible polymer substrate. J. Adhes. Sci. Technol. 26 (20—21), 2393–2404. https://doi.org/10.1163/156856111X599526.

Keunun, P., Rakkarn, T., Yunu, T., Paichid, N., Prasertsan, Poonsuk, Sangkharak, Kanokphorn, 2018. The production of polyhydroxybutyrate by two-step fermentation and the application of polyhydroxybutyrate as a novel substrate for a biolubricant. J. Polym. Environ. 26, 2459–2466. https://doi.org/10.1007/s10924-017-1140-0.

Khosravi-Darani, K., Bucci, D.Z., 2015. Application of poly(hydroxyalkanoate) in food packaging: improvements by nanotechnology. Chem. Biochem. Eng. Q. 29 (2), 275–285. https://doi.org/10.15255/CABEQ.2014.2260.

Kiran Purama, R., Al-Sabahi, J.N., Sudesh, K., 2018. Evaluation of Date Seed Oil and Date Molasses as Novel Carbon Sources for the Production of Poly(3Hydroxybutyrate-co-3Hydroxyhexanoate) by Cupriavidus Necator H16 Re 2058/pCB113. https://doi.org/10.1016/j.indcrop.2018.04.013.

Koller, M., 2017. Advances in Polyhydroxyalkanoate (PHA) Production, Advances in Polyhydroxyalkanoate (PHA) Production. MDPI, Bioengineering. https://doi.org/10.3390/books978-3-03842-636-3.

Kookos, I.K., Koutinas, A., Vlysidis, A., 2019. Life Cycle Assessment of Bioprocessing Schemes for Poly(3-hydroxybutyrate) Production Using Soybean Oil and Sucrose as Carbon Sources. https://doi.org/10.1016/j.resconrec.2018.10.025.

Kourmentza, C., Plácido, J., Venetsaneas, N., Burniol-Figols, A., Varrone, C., Gavala, H.N., Reis, M.A.M., 2017. Recent advances and challenges towards sustainable polyhydroxyalkanoate (PHA) production. Bioengineering. MDPI AG https://doi.org/10.3390/bioengineering4020055.

Leong, Y.K., Pau, Show, L., John, Lan, C.-W., Loh, H.-S., Hon, Lam, L., Tau, Ling, C., Show, P.L., 2017. Economic and environmental analysis of PHAs production process. Clean Techn. Environ. Policy 19, 1941–1953. https://doi.org/10.1007/s10098-017-1377-2.

Levasseur, A., Cavalett, O., Fuglestvedt, J.S., Gasser, T., Johansson, D.J.A., Jørgensen, S.V., Raugei, M., Reisinger, A., Schivley, G., Strømman, A., Tanaka, K., Cherubini, F., 2016. Enhancing life cycle impact assessment from climate science: review of recent findings and recommendations for application to LCA. Ecol. Indic. 71, 163–174. https://doi.org/10.1016/j.ecolind.2016.06.049 Elsevier Ltd.

Maga, D., Hiebel, M., Thonemann, N., 2019. Life cycle assessment of recycling options for polylactic acid. Resour. Conserv. Recycl. 149, 86–96. https://doi.org/10.1016/j.resconrec.2019.05.018 Elsevier B.V..

Meereboer, K.W., Misra, M., Mohanty, A.K., 2020. Review of recent advances in the biodegradability of polyhydroxyalkanoate (PHA) bioplastics and their composites. Green Chem. 22 (17), 5519–5558. https://doi.org/10.1039/d0gc01647k Royal Society of Chemistry.

Moretto, G., Lorini, L., Pavan, P., Crognale, S., Tonanzi, B., Rossetti, S., Majone, M., Valentino, F., 2020. Biopolymers from urban organic waste: influence of the solid retention time to cycle length ratio in the enrichment of a Mixed Microbial Culture (MMC). ACS Sustain. Chem. Eng. 8 (38), 14531–14539. https://doi.org/10.1021/acssuschemeng.0c04980 American Chemical Society.

Ögmundarson, Ó., Sukumara, S., Laurent, A., Fantke, Peter, 2020. Environmental hotspots of lactic acid production systems. 12, 19–38. https://doi.org/10.1111/gcbb.12652.

Owsianiak, M., Ryberg, M.W., Renz, M., Hitzl, M., Hauschild, M.Z., 2016. Environmental performance of hydrothermal carbonization of four wet biomass waste streams at industry-relevant scales. ACS Sustain. Chem. Eng. 4 (12), 6783–6791. https://doi.org/10.1021/acssuschemeng.6b01732.

Pavan, F.A., Junqueira, T.L., Watanabe, M.D.B., Bonomi, A., Quines, L.K., Schmidell, W., De Aragao, G.M.F., 2019. Economic Analysis of Polyhydroxybutyrate Production by Cupriavidus Necator Using Different Routes for Product Recovery. https://doi.org/10.1016/j.bej.2019.03.009.

Rameshkumar, S., Shaiju, P., O'connor, K.E., Babu, R., 2020. Bio-based and Biodegradable Polymers-state-of-the-art, Challenges and Emerging Trends. https://doi.org/10.1016/j.cogsc.2019.12.005.

Remor Dalsasso, R., Andre Pavan, F., Emilio Bordignon, S., Maria Falcão de Aragão, G., Poletto, P., 2019. Polyhydroxybutyrate (PHB) Production by Cupriavidus Necator From Sugarcane Vinasse and Molasses as Mixed Substrate. https://doi.org/10.1016/j.procbio.2019.07.007.

Rossi, V., Cleeve-Edwards, N., Lundquist, L., Schenker, U., Dubois, C., Humbert, S., Jolliet, O., 2015. Life cycle assessment of end-of-life options for two biodegradable packaging materials: sound application of the European waste hierarchy. J. Clean. Prod. 86, 132–145. https://doi.org/10.1016/j.jclepro.2014.08.049 Elsevier Ltd.

Ryberg, M.W., Hauschild, M.Z., Wang, F., Averous-Monnery, S., Laurent, A., 2019. Global environmental losses of plastics across their value chains. Resour. Conserv. Recycl. 151, 104459. https://doi.org/10.1016/j.resconrec.2019.104459 Elsevier B.V..

Schowanek, D., Borsboom-Patel, T., Bouvy, A., Colling, J., de Ferrer, J.A., Eggers, D., Groenke, K., Gruenenwald, T., Martinsson, J., Mckeown, P., Miller, B., Moons, S., Niedermann, K., Pérez, M., Schneider, C., Viot, J.F., 2018. New and updated life cycle inventories for surfactants used in European detergents: summary of the ERASM surfactant life cycle and ecofootprinting project. Int. J. Life Cycle Assess. 23 (4), 867–886. https://doi.org/10.1007/s11367-017-1384-x The International Journal of Life Cycle Assessment.

Shine, K.P., Fuglestvedt, J.S., Hailemariam, K., Stuber, N., 2005. Comparing climate impacts of emissions of greenhouse gases. Climate Change 68 (2005), 281–302.

Spierling, S., Knüpffer, E., Behnsen, H., Mudersbach, M., Krieg, H., Springer, S., Albrecht, S., Herrmann, C., Endres, H.J., 2018. Bio-based plastics - a review of environmental, social and economic impact assessments. J. Clean. Prod. 185, 476–491. https://doi.org/10.1016/j.jclepro.2018.03.014 Elsevier Ltd.

Spierling, S., Venkatachalam, V., Mudersbach, M., Becker, N., Herrmann, C., Endres, H.J., 2020. End-of-life options for bio-based plastics in a circular economy-status quo and potential from a life cycle assessment perspective. Resources, 90 https://doi.org/10.3390/RESOURCES9070090 MDPI AG.

Struller, C.F., Kelly, P.J., Copeland, N.J., 2014. Aluminum oxide barrier coatings on polymer films for food packaging applications. Surf. Coat. Technol. 241, 130–137. https://doi.org/10.1016/j.surfcoat.2013.08.011.

Takriti, S.E., Searle, S., Pavlenko, N., 2017. Indirect Greenhouse Gas Emissions of Molasses Ethanol in the European Union, International Council on Clean Transportation.

Troschl, C., Meixner, K., Fritz, I., Leitner, K., Romero, A.P., Kovalcik, A., Sedlacek, P., Drosg, B., 2018. Pilot-scale production of poly-β-hydroxybutyrate with the cyanobacterium Synechocytis sp. CCALA192 in a non-sterile tubular photobioreactor. Algal Res. 34, 116–125. https://doi.org/10.1016/j.algal.2018.07.011 Elsevier B.V..

Wongsirichot, P., Gonzalez-Miquel, M., Winterburn, J., 2020. Integrated biorefining approach for the production of polyhydroxyalkanoates from enzymatically hydrolyzed rapeseed meal under nitrogen-limited conditions. ACS Sustain. Chem. Eng. 8 (22), 8362–8372. https://doi.org/10.1021/acssuschemeng.0c02406.

Yamane, T., 1993. 'Yield of poly-D(-)-3-hydroxybutyrate from various carbon sources: a theoretical study'. Biotechnol. Bioeng. 41 (1), 165–170. https://doi.org/10.1002/bit.260410122.